nature communications

Article

https://doi.org/10.1038/s41467-026-69126-4

Engineered bacterial therapy suppresses Enterohemorrhagic *Escherichia coli* through metabolic competition and virulence silencing

Received: 8 June 2025

Accepted: 26 January 2026

Published online: 03 February 2026

Check for updates

Guozhen Ma[1,2,3,4,9], Ruiying Liu[4,9], Xueping Li[5,9], Jialin Wu[6,9], Yuanyuan Niu[4], Sheng Wang[5], Ziwei Chen[5], Xudong Qin[5], Qian Wang[4], Junyue Wang[7], Jiamin Qian[4], Mingqing Zhang[8], Yu Pang[4], Yamin Sun[1,2,3] ✉, Guosheng Tang[6] ✉, Tao Wang[5] ✉ & Yutao Liu[1,2,3] ✉

Enterohemorrhagic *Escherichia coli* (EHEC) is a severe foodborne pathogen that can lead to hemolytic uremic syndrome. However, antibiotics are contraindicated for EHEC treatment due to toxin release and gut microbiota disruption. Here we report a dual-mechanism therapeutic strategy combining an engineered *Escherichia coli* Nissle 1917 strain (EcN3) with 2′-fucosyllactose (2-FL) delivered via multicompartment microspheres (MCMs). EcN3 expresses α-L-fucosidase to hydrolyze 2-FL into lactose and fucose. Lactose enhances glucuronic acid utilization, limiting a preferred nutrient of EHEC, whereas fucose activates FusKR signaling to suppress virulence gene expression. MCMs confer gastric protection and enable targeted colonic release, ensuring coordinated activity. In female mouse models and infant rabbit models of *Citrobacter rodentium* and EHEC infection, this system reduces intestinal colonization, virulence gene expression and epithelial damage without inducing Shiga toxin production. Moreover, MCMs-based strategy preserves the relative abundance of *Lactobacillus*, and promotes intestinal integrity. This targeted strategy presents a viable alternative to antibiotics, addressing EHEC pathogenesis and antibiotic resistance.

The threat of bacterial infections continues to escalate globally, with the World Health Organization (WHO) projecting that by 2050, these infections may claim up to 10 million lives annually, surpassing the mortality rate of cancer[1]. Enterohemorrhagic *Escherichia coli* (EHEC) is a major foodborne pathogen with significant health risks worldwide[2]. EHEC infection has the potential to result in life-threatening complications, notably hemolytic uremic syndrome (HUS), which is characterized by acute renal failure, hemolytic anemia, and thrombocytopenia[3]. These severe outcomes highlight the critical need for a comprehensive understanding of EHEC pathogenic mechanisms

[1]National Key Laboratory of Intelligent Tracking and Forecasting for infectious Diseases, Beijing Ditan Hospital, Capital Medical University, Beijing, China. [2]Beijing Institute of Infectious Diseases, Beijing, China. [3]National Center for Infectious Diseases, Beijing Ditan Hospital, Capital Medical University, Beijing, China. [4]TEDA Institute of Biological Sciences and Biotechnology, Nankai University, Tianjin, China. [5]School of Life Sciences, Tianjin University, Tianjin, China. [6]Guangzhou Municipal and Guangdong Provincial Key Laboratory of Molecular Target & Clinical Pharmacology, School of Pharmaceutical Sciences, Guangzhou Medical University, Guangzhou, Guangdong, P. R. China. [7]Academy of Medical Engineering and Translational Medicine, Tianjin University, Tianjin, China. [8]The Institute of Translational Medicine, Tianjin Union Medical Center of Nankai University, Nankai University, Tianjin, China. [9]These authors contributed equally: Guozhen Ma, Ruiying Liu, Xueping Li, Jialin Wu. ✉e-mail: nksunyamin@aliyun.com; guoshengtang@gzhmu.edu.cn; wangtaobio@tju.edu.cn; liuyutao623@163.com

and the development of effective therapeutic strategies. Although antibiotics are generally effective in eradicating bacterial pathogens, their use in treating EHEC infections is contraindicated due to the risk of exacerbating severe symptoms by releasing toxins[4]. Meanwhile, the broad-spectrum activity of most antibiotics can significantly disrupt the intestinal microbiota, resulting in dysbiosis, which has been linked to heightened disease risks[5]. Consequently, there is an urgent need to develop therapeutic interventions for EHEC infections.

The pathogenic process of EHEC infection involves several complex mechanisms, among which the Shiga toxins (Stxs) and the locus of enterocyte effacement (LEE) island play pivotal roles[6]. The LEE Island harbors multiple genes associated with EHEC pathogenicity, including those encoding the proteins necessary for the assembly and function of T3SS, leading to the formation of attaching and effacing (A/E) lesions on intestinal epithelial cells, which is a hallmark of EHEC pathogenesis[7]. The formation of A/E lesions involves the direct injection of effector proteins (such as Tir and EspB) into host cells by T3SS, which triggers the rearrangement of the host cell cytoskeleton, primarily manifested by the polymerization of actin and the formation of actin pedestals beneath the cell membrane[8,9]. This cytoskeletal rearrangement stabilizes the binding of bacteria to host cells. It leads to the destruction of microvilli and the shedding of intestinal epithelial cells, compromising the intestinal barrier function and promoting bacterial colonization and toxin release[10]. This series of events ultimately exacerbates intestinal inflammation and tissue damage by EHEC.

Citrobacter rodentium (*C. rodentium*) is a Gram-negative, mouse-restricted enteric pathogen that causes transmissible colonic hyperplasia and forms A/E lesions in the intestinal epithelium of mice[11]. *C. rodentium* serves as a widely used surrogate model for studying the pathogenesis of clinically significant human pathogens, particularly EHEC and enteropathogenic *E. coli* (EPEC), as they share similar key virulence factors and LEE pathogenicity island[12,13]. The core of this similarity is in the presence of the LEE, a ~35-Kb pathogenicity island conserved among *C. rodentium*, EPEC, and EHEC. The LEE encodes a type III secretion system (T3SS), the adhesin intimin, its translocated receptor Tir, as well as a suite of effectors essential for colonization and A/E lesion formation[12]. In both humans and mice, these effectors mediate not only bacterial adherence but also subversion of host cell signaling and immune response modulation.

EHEC employs complex mechanisms to adapt to the host environment during infection, facilitating successful infection and colonization. Initially, EHEC effectively senses and responds to various intestinal metabolite signals, including riboflavin and fucose, critical factors regulating the expression of its type III secretion system (T3SS)[14,15]. Additionally, EHEC exhibits distinct metabolic capabilities, utilizing carbon sources such as glucuronic acid (GlcA) and galacturonic acid (GalA), which differ from those preferred by commensal gut bacteria. This unique metabolic flexibility significantly enhances its growth competitiveness and survival within the complex gut environment[16,17]. Furthermore, EHEC infection actively disrupts the gut microbiota, altering microbial composition and metabolic activity. This microbiome dysbiosis promotes EHEC colonization, favoring pathogen dominance and persistence in the intestinal niche[18]. Given these multifaceted pathogenic strategies, simultaneously targeting multiple critical pathways represents a promising therapeutic approach to substantially mitigate EHEC pathogenicity in the host. However, currently available therapies cannot generally concurrently address these diverse infection mechanisms. Therefore, developing strategies simultaneously targeting multiple pathogenic mechanisms holds significant potential for improving therapeutic outcomes against EHEC infections.

Microgels can be engineered with tailored biodegradability, excellent permeability to oxygen and other soluble factors, and robust mechanical stability, making them highly advantageous for applications in tissue engineering and drug delivery[19–21]. Advancements in biomaterials have recently facilitated the development of multicompartment microspheres (MCMs), mimicking the compartmentalized structures naturally found in eukaryotic cells[22]. Furthermore, a scalable, oil-free technique known as “gas-shearing”, which utilizes gas-flow-assisted microdroplet formation, enables the precise and efficient production of monodisperse multicompartment microspheres. These microspheres allow exact control over individual compartment characteristics and thus offer notable benefits for biomedical usage, such as precise regulation of payload release kinetics, safeguarding sensitive components against harsh gastrointestinal conditions, and targeted delivery to specific intestinal regions[23–26]. Importantly, MCMs possess the potential to simultaneously encapsulate multiple therapeutic agents, facilitating coordinated targeting of diverse pathogenic mechanisms employed by pathogens- a significant advantage given that EHEC typically activates several parallel virulence strategies during infection[27].

In this study, we engineer an EcN-based therapeutic system combining metabolic interference and virulence suppression to combat EHEC infections. The engineered EcN3 strain integrates EHEC-derived glucuronate utilization genes (*uxaC*/*uxuB*/*uxuA*) under a lactose-inducible promoter, and an α-L-fucosidase (FucA), regulated by the PfnrS promoter, which cleaves 2′-fucosyllactose (2-FL) into lactose and fucose. The resultant lactose induces GlcA catabolic gene expression to compete for interception of EHEC’s preferred carbon source (GlcA) in the large intestine. Concurrently, the resultant fucose suppresses EHEC virulence by activating the FusKR two-component system, effectively silencing LEE pathogenicity island genes. To enhance the preventive efficacy of this system, we develop multicompartment microspheres (MCMs) containing EcN3 and 2-FL, which shield these components from gastric degradation and ensure targeted release in the large intestine. This integrated approach achieves pathogen inhibition through spatiotemporal coordination of carbon source depletion, virulence gene silencing, and microbiome-compatible delivery, establishing a targeted alternative to broad-spectrum antibiotics.

Results

Design and characterization of 2-FL- responsive engineered bacteria

To against EHEC infections, we chose *Escherichia coli* Nissle 1917 (EcN) as a chassis strain due to its long-standing safety record in humans and widespread application in microbial engineering therapies[28]. Previous research confirmed that glucuronic acid (GlcA) confers a competitive advantage for EHEC expansion through its utilization as a carbon source[16]. So, we employed a carbon source competition strategy to inhibit EHEC infection. Specifically, the *uxaC*, *uxuB*, and *uxuA* genes from EHEC were cloned into a pACYC plasmid under the control of a constitutive J23100 promoter and transformed into EcN, resulting in the engineered strain EcN1. Growth analysis demonstrated that EcN1 exhibited a higher optical density (OD_{600}) than wild-type EcN when cultured in M9 medium with GlcA as the sole carbon source (Supplementary Fig. 1a). Additionally, high-performance liquid chromatography (HPLC) analysis revealed that, during an 8-hour incubation period, the GlcA metabolic rate of EcN1 was 13.17% higher than that of EcN (Supplementary Fig. 1b). These results indicate that the overexpression of *uxaC*, *uxuB*, and *uxuA* significantly enhances GlcA utilization in vitro.

To enhance the response ability of EcN1 in the intestinal environment, a lactose-inducible promoter was used to replace the constitutive promoter, thus constructing EcN2. Growth analysis indicates that EcN2 demonstrates a higher OD_{600} compared to EcN in M9 medium supplemented with GlcA and IPTG (Supplementary Fig. 1c). Quantitative reverse transcription PCR (qRT-PCR) analysis confirmed that the expression of the *uxaC*, *uxuB*, and *uxuA* in EcN2 was

https://doi.org/10.1038/s41467-026-69126-4

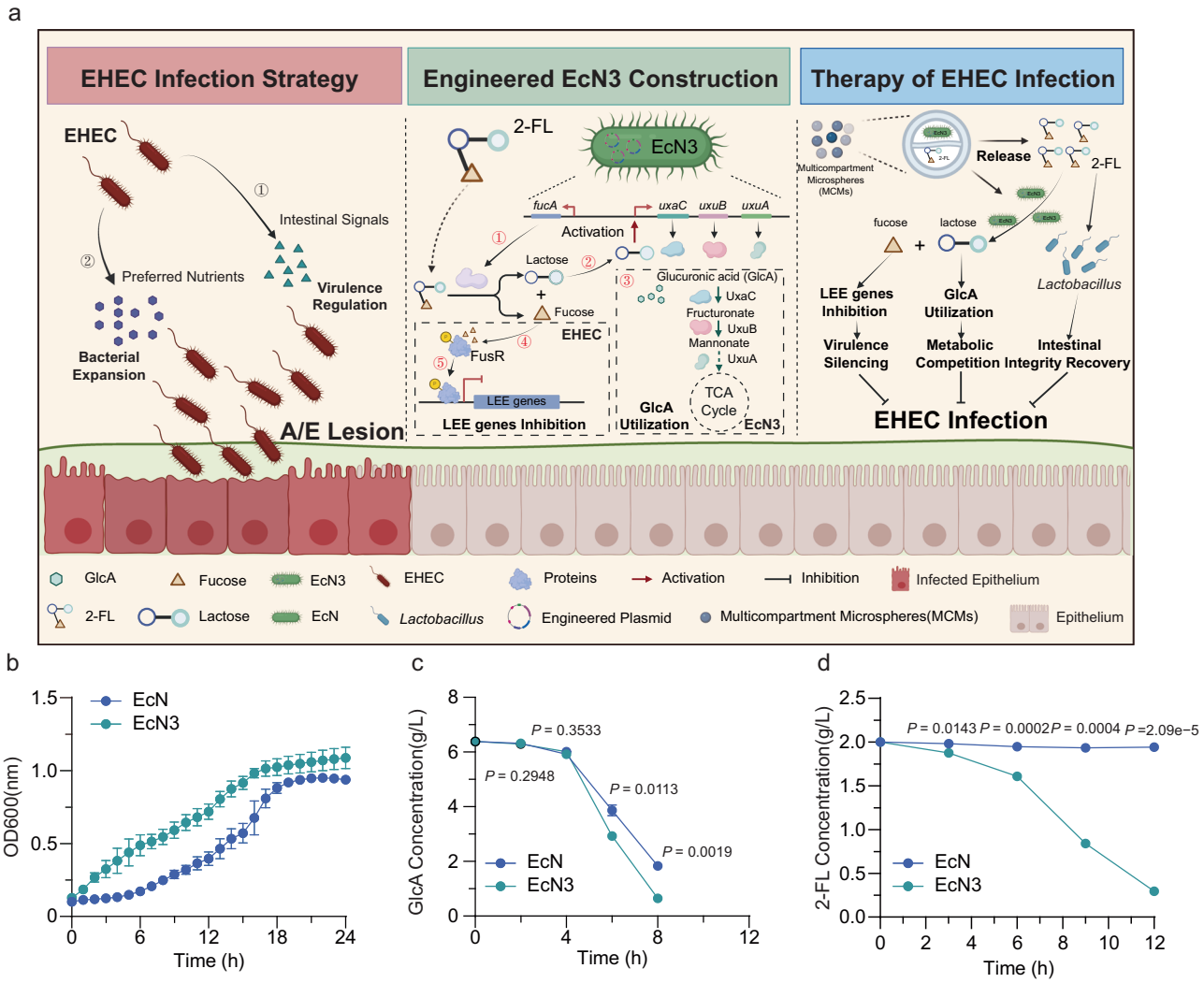

Fig. 1 | Design and characterization of 2-FL-degrading engineered bacteria. **a** Schematic of the construction process for 2-FL-degrading engineered bacteria EcN3 and therapy strategy of E/H-MCMs (Created in https://BioRender.com). **b** Growth curves of EcN3 and EcN in M9 medium supplemented with 2-FL and GlcA ($n = 3$ independent experiments). **c**, **d** HPLC quantification of GlcA (**c**) and 2-FL (**d**) consumption by EcN3 or EcN cultured in M9 medium supplemented with 2-FL and GlcA ($n = 3$ independent experiments). Significance was determined by a two-tailed unpaired Student's *t*-test (**c**, **d**) and indicated as the *P* value. $^{*}P < 0.05$, $^{**}P < 0.01$, $^{***}P < 0.001$; ns no significant difference. Data were presented as mean ± s.d. **b**–**d** Source data are included in the Source Data file.

significantly upregulated in M9 medium supplemented with GlcA and IPTG (Supplementary Fig. 1d). Furthermore, HPLC analysis demonstrated that EcN2 utilized GlcA more efficiently than EcN, exhibiting a 23.9% increase in the GlcA metabolism. (Supplementary Fig. 1e).

Given the toxicity of IPTG to hosts[29], a host-friendly inducible system was developed. We selected 2-FL, a human milk oligosaccharide that can be hydrolyzed by FucA into lactose and fucose, as an alternative inducer. To construct this regulatory system, we screened for high-efficiency FucA capable of hydrolyzing 2-FL were screened. Genes encoding α-L-fucosidase (FucA) from *Xanthomonas euvesicatoria*, *Paenibacillus thiaminolyticus*, *Bifidobacterium longum*, and *Thermotoga maritima*, under the control of the PfnrS promoter, were cloned into the pACYC plasmids and introduced into EcN, resulting in strains EcN-Xe, EcN-Pt, EcN-Bl, and EcN-Tm. Growth analysis revealed that EcN-Tm utilized 2-FL most efficiently, exhibiting the highest OD600 under identical conditions (Supplementary Fig. 1f). Then, we recombined the PfnrS-driven *fucA* from *Thermotoga maritima* into the plasmid carried by EcN2 to obtain EcN3 (Fig. 1a). Growth and HPLC analyses demonstrated that EcN3 exhibited enhanced growth and more efficient utilization of both GlcA and 2-FL in M9 medium supplemented with these substrates, compared to EcN (Fig. 1b–d and Supplementary Fig. 1g, h).

To evaluate whether EcN3 could effectively utilize GlcA in vivo, mice were orally administered EcN3 following treatment with either 2-FL or galactooligosaccharides (GOS, negative control). After 8 h post-treatment, qRT-PCR analysis indicated that the expression levels of *uxaC*, *uxuB*, *uxuA*, and *fucA* in 2-FL-treated mice were 9.25 to 12.59-fold higher than those in GOS-treated mice (Supplementary Fig. 1i). Further results showed that the GlcA level in 2-FL-treated mice were significantly lower than that in GOS-treated mice (Supplementary Fig. 1j). The result suggests that EcN3 effectively metabolizes 2-FL in vivo, activating GlcA utilization genes in mice colon.

The combination of EcN3 and 2-FL inhibits EHEC growth and virulence

Previous results confirmed that EcN3 has confirmed GlcA utilization and 2-FL degradation capacities. We further investigate whether EcN3 can inhibit the growth and virulence of EHEC in vitro. First, the competitive growth assays were conducted. In M9 medium supplemented with GlcA and GOS, the competitive index (CI) values of EcN and EcN3

https://doi.org/10.1038/s41467-026-69126-4

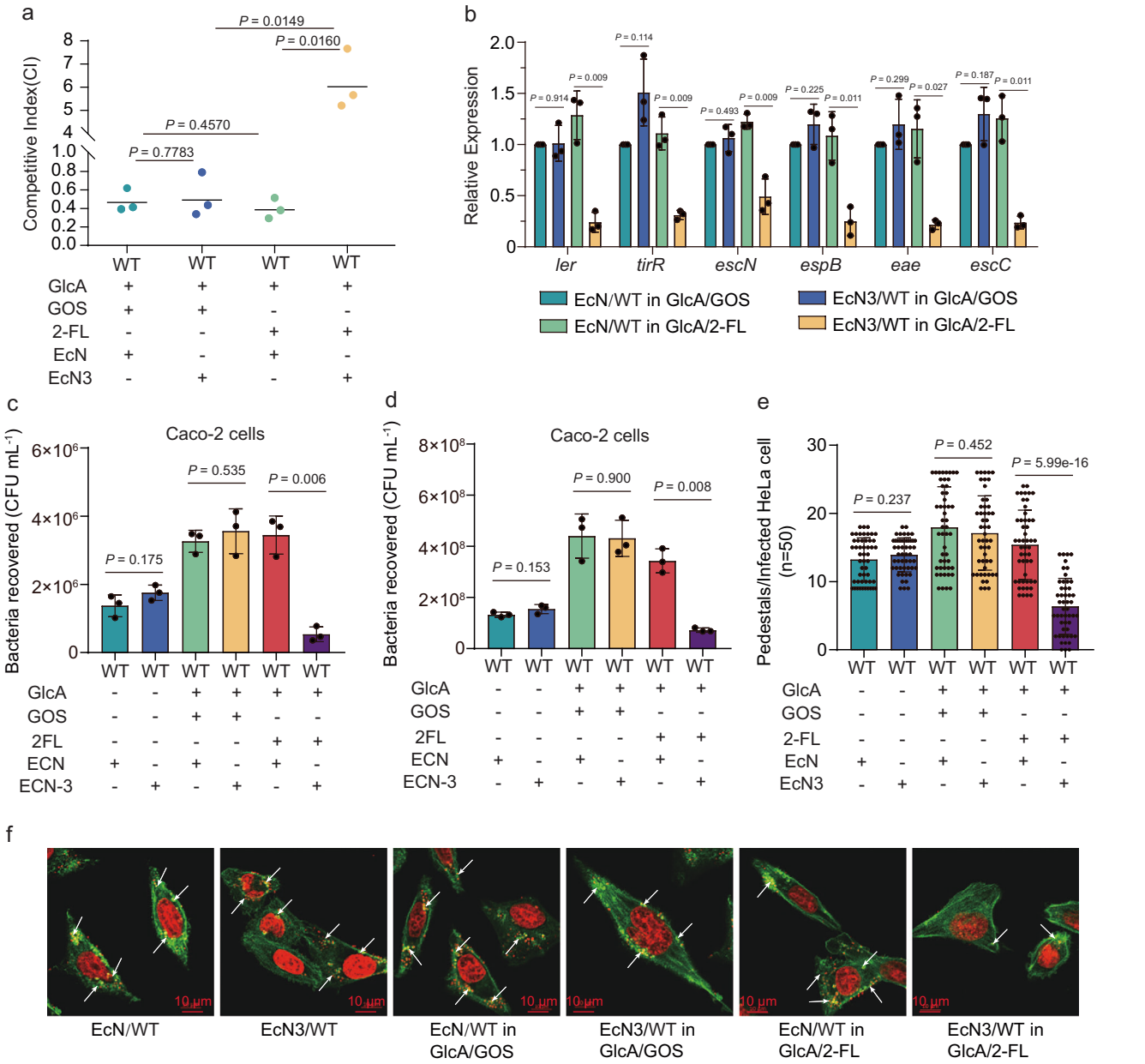

Fig. 2 | The combination of EcN3 and 2-FL inhibits EHEC growth and virulence in vitro. a Competitive index of EcN/WT and EcN3/WT in M9 medium supplemented with GlcA and GOS or 2-FL ($n = 3$ independent experiments). Horizontal bars indicate the median. **b** qRT-PCR analysis of LEE gene expression of WT co-cultured with EcN or EcN3 in DMEM supplemented with GlcA and GOS or 2-FL ($n = 3$ independent experiments). **c** Adherence of WT to Caco-2 cells co-cultured with EcN or EcN3 in DMEM medium supplemented with GlcA and GOS or 2-FL ($n = 3$ independent experiments). **d** The survival of WT in Caco-2 cells culture supernatants co-cultured with EcN or EcN3 in DMEM medium supplemented with GlcA and GOS or 2-FL ($n = 3$ independent experiments). **e**, **f** FAS assay quantification of the number (**e**) and representative images (**f**) of pedestals per infected cell infected with WT co-cultured with EcN or EcN3, in DMEM medium supplemented with GlcA and GOS or 2-FL ($n = 50$ cells). The actin cytoskeleton (green) and nuclei of HeLa cells and bacteria (red) are shown. Arrowheads indicate the pedestals. Scale bar, 10 μm. Significance was determined by a two-tailed unpaired Student's *t*-test (**a**–**e**) and indicated as the *P* value. $^{*}P < 0.05$, $^{**}P < 0.01$, $^{***}P < 0.001$; ns no significant difference. Data were presented as mean ± s.d. (**b**–**e**). Source data are included in the Source Data file.

against wild-type EHEC (WT) were 0.47 and 0.52, respectively (Fig. 2a). However, when M9 medium supplemented with both GlcA and 2-FL, the CI values of EcN and EcN3 against WT were 0.40 and 6.08, respectively (Fig. 2a). These results demonstrate that EcN3 exhibits a significant competitive advantage in the presence of GlcA and 2-FL, effectively inhibiting the survival of EHEC in vitro.

To further elucidate whether the combination of EcN3 and 2-FL modulates the inhibition of EHEC virulence gene expression, qRT-PCR experiments were performed. When WT was co-cultured with EcN in DMEM supplemented with GlcA and GOS, the expression of LEE genes was comparable to those observed in WT co-cultured with EcN3 under identical conditions (Fig. 2b). However, WT co-culture with EcN3 in DMEM supplemented with GlcA and 2-FL resulted in a significant reduction of LEE genes expression compared to WT co-culture with EcN (Fig. 2b). These findings indicate that 2-FL acts synergistically with EcN3 to suppress the LEE genes expression of EHEC in vitro effectively. Then, the effect of the combination of EcN3 and 2-FL on bacterial adherence was analyzed. The HeLa and Caco-2 cells were infected with

WT in the presence of EcN or EcN3, supplemented with GlcA and GOS or 2-FL. The results revealed no significant difference in bacterial adherence between WT co-cultured with EcN or EcN3 in the untreated and GOS-treated groups (Fig. 2c and Supplementary Fig. 2a). However, WT co-cultured with EcN3 exhibited an 11.88-fold reduction in cell adherence compared to WT co-cultured with EcN in the 2-FL-treated group (Fig. 2c and Supplementary Fig. 2a). In addition, the bacteria number in cell culture supernatants of each group was analyzed, which showed consistent results (Fig. 2d and Supplementary Fig. 2b). Furthermore, fluorescent actin staining (FAS) analysis demonstrated that the formation of actin pedestals per infected cell was 2.41 to 2.81-fold lower in the EcN3 supplemented with both GlcA and 2-FL compared to the EcN, the EcN/2-FL, and EcN3/2-FL groups (Fig. 2e, f). These results indicate that EcN3, combined with GlcA and 2-FL, significantly reduces EHEC's adherence and actin pedestal formation capability in vitro.

Given that the combination of EcN3 and 2-FL confers a competitive advantage over EHEC via nutrient deprivation, we considered whether starvation-induced stress might activate Stx phages and increase Stx production, similar to the effect of antibiotics. To address this, we analysis the impact of EcN3 and 2-FL on Stxs expression and release. qRT-PCR showed that, when WT EHEC was co-cultured with EcN3 in DMEM supplemented with GlcA and 2-FL or GOS, the expression of *stx2a* was not significantly altered compared with WT co-cultured with EcN supplemented with GlcA and 2-FL or GOS (Supplementary Fig. 2c). Consistently, ELISA indicated no change in Stxs release under the same conditions (Supplementary Fig. 2d). These data suggest that the combination of EcN3 and 2-FL does not enhance Stx production during GlcA competition.

The combination of EcN3 and 2-FL inhibits EHEC growth and virulence through two distinct pathways

Given that the *uxuB* gene encodes an enzyme involved explicitly in GlcA catabolism, we investigated whether EcN3 inhibits EHEC growth through the *uxuB*-mediated metabolic pathway. To test this hypothesis, we constructed a mutant of *uxuB* in EHEC (Δ*uxuB*) and performed competitive growth assays in M9 medium supplemented with glucose or GlcA. In M9 medium with glucose and in DMEM medium, there was no significant competitive difference between Δ*uxuB* and the WT. However, in M9 medium supplemented with GlcA, Δ*uxuB* showed a threefold reduction in growth, indicating that loss of *uxuB* does not affect growth under general conditions but specifically impairs growth when GlcA is the sole carbon source (Supplementary Fig. 3a). Furthermore, competitive assays pairing EcN3 with either WT or Δ*uxuB* in M9 medium containing GlcA and GOS or 2-FL showed that EcN3 significantly inhibited WT growth in the presence of 2-FL and GlcA (Fig. 3a). However, the Δ*uxuB* exhibited similar growth suppression by EcN3 in the presence or absence of 2-FL (Fig. 3a). qRT-PCR analysis revealed that LEE gene expression in both WT and Δ*uxuB* were reduced when co-cultured with EcN3 and 2-FL in DMEM compared to GOS controls (Fig. 3b). However, LEE gene expression showed no significant difference between WT and Δ*uxuB* in presence of EcN3 and 2-FL (Fig. 3b). These data demonstrate that *uxuB* deletion specifically abolishes growth competition without influencing virulence genes expression.

Previous research confirmed that EHEC senses fucose to inhibit LEE gene expression through the two-component system FusKR[15]. We investigated whether the combination of EcN3 and 2-FL suppresses EHEC virulence via the FusKR-mediated pathway. qRT-PCR analysis revealed that in the Δ*fusKR*, co-culture with EcN3 in DMEM supplemented with 2-FL or GOS failed to inhibit LEE gene expression (Fig. 3c). In contrast, under the same conditions, the WT exhibited a significant reduction in LEE gene expression in the presence of 2-FL (Fig. 3c). Consistent with these findings, bacterial adherence assays demonstrated that the Δ*fusKR* mutant co-cultured with EcN3 and 2-FL showed no significant reduction in adherence compared to the Δ*fusKR* mutant co-cultured with EcN3 and GOS in HeLa and Caco-2 cells (Fig. 3d and Supplementary Fig. 3b). However, the WT strain displayed a decrease in adherence in the presence of EcN3 and 2-FL (Fig. 3d and Supplementary Fig. 3b). In addition, the growth of WT co-cultured with EcN3 and 2-FL in cell culture supernatants was significantly reduced compared with other groups (Fig. 3e and Supplementary Fig. 3c). Similarly, FAS analysis indicated that the actin pedestal formation per infected cell remained unchanged in the Δ*fusKR* under these conditions (Fig. 3f, g). Conversely, the WT strain exhibited a significant reduction in actin pedestal formation in the presence of EcN3 and 2-FL (Fig. 3f, g). In addition, the competitive growth assays of WT and Δ*fusKR* in M9 medium supplemented with glucose or GlcA, as well as in DMEM medium. The results showed that under all three conditions, the Δ*fusKR* mutation did not affect growth (Supplementary Fig. 3d). These results suggest that the EcN3-degraded fucose inhibits LEE gene expression and bacterial adherence by activating the FusKR pathway.

Collectively, these findings demonstrate that in the presence of 2-FL and EcN3, the expression of *uxaC*, *uxuB*, and *uxuA* in EcN3 was activated, thereby inhibiting the growth of EHEC through GlcA competition. In parallel, the expression of LEE virulence genes was inhibited through activation of the FusKR. These dual mechanisms ultimately lead to concurrent restriction of EHEC growth and virulence in vitro.

Therapeutic effect of the combination EcN3 and 2-FL against *C. rodentium* and EHEC by inhibiting its survival and virulence during infection

To investigate the therapeutic effect of the EcN3 and 2-FL combination on EHEC infection in vivo, we performed infant rabbit colonization experiments using EHEC O157:H7 strain EDL933 (Fig. 4a). Compared with the EcN/GOS, EcN/2-FL, and EcN3/GOS groups, treatment with EcN3/2-FL resulted in a significant reduction in both luminal survival and intestinal tissue colonization in the colons of infant rabbits (Fig. 4b, c). In vivo RT-PCR analysis also showed that LEE genes were significantly downregulated when rabbit treated with EcN3/2-FL (Fig. 4d). However, expression of *stx2a* did not differ among the groups, indicating that EcN3/2-FL does not suppress Stx expression (Fig. 4d). Then, we quantified Stx levels in luminal contents by ELISA. The results showed that Stx levels were significantly lower in the EcN3/2-FL group compared with the EcN/GOS, EcN/2-FL, and EcN3/GOS groups (Fig. 4e), suggesting that the reduced toxin levels are not due to transcriptional regulation but are more likely a consequence of decreased bacterial luminal survival and intestinal tissue colonization.

We next used *C. rodentium*, a murine pathogen that serves as a surrogate model for EHEC infection (Fig. 4a), to validate these findings. Mice infection assays of *C. rodentium* demonstrated that administration of the combination of EcN3 and 2-FL significantly inhibited the luminal content survival and intestinal tissue colonization of *C. rodentium* compared to the EcN/GOS group, EcN/2-FL group, and EcN3/GOS group (Fig. 4f, g). Additionally, qRT-PCR analysis revealed that the expression of LEE genes of *C. rodentium* was significantly downregulated by 3.4 to 5.1-fold in the EcN3/2-FL group in the colon (Fig. 4h). In contrast, compared with the EcN/GOS group, the EcN/2-FL group, and the EcN3/GOS group did not result in a direct downregulation of LEE gene expression (Fig. 4h). These data indicate that administration of the combination of EcN3 and 2-FL effectively reduces the intestinal survival and virulence gene expression in vivo.

Intestinal colonization by *C. rodentium* induces gut inflammation and lethality, characteristic features of diseases caused by *C. rodentium* in hosts[30,31]. To investigate the influence of the combination of EcN3 and 2-FL on the pathogenicity of *C. rodentium*, we monitored the lethality and histological damage in infected mice. The lethality curves demonstrated that mice of the EcN3/2-FL group exhibited reduced mortality compared to those in the EcN/GOS, EcN/2-FL, and EcN3/GOS groups (Fig. 4i). We also evaluated histological damage in the colon of

https://doi.org/10.1038/s41467-026-69126-4

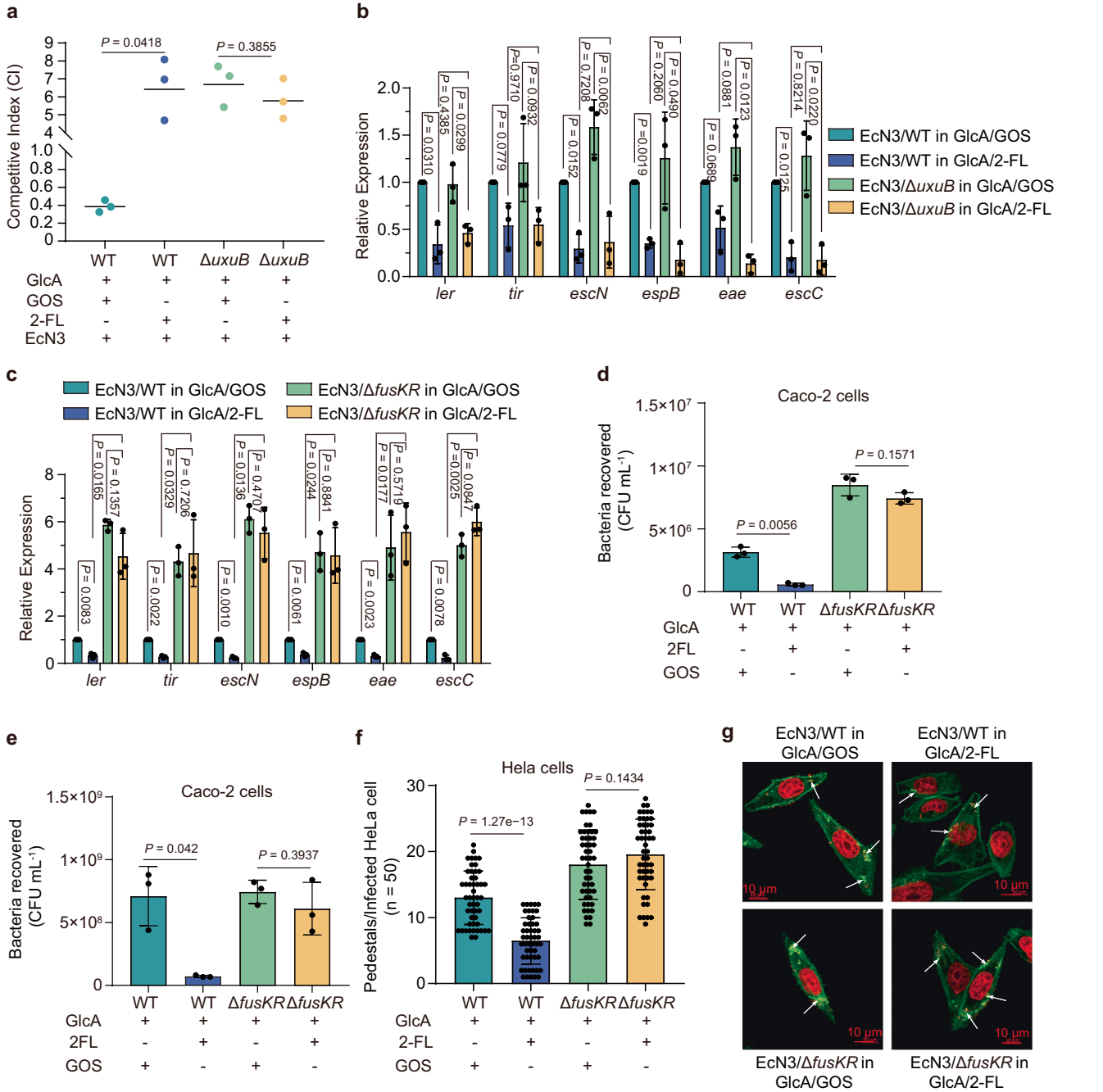

Fig. 3 | The combination of EcN3 and 2-FL inhibits EHEC growth and virulence through two distinct pathways. a Competitive index of EcN3/WT and EcN3/Δ*uxuB* in DMEM medium supplemented with GlcA and GOS or 2-FL ($n = 3$ independent experiments). Horizontal bars indicate the median. **b** qRT-PCR analysis of LEE gene expression in WT or Δ*uxuB*, co-cultured with EcN3 in DMEM supplemented with GlcA and GOS or 2-FL ($n = 3$ independent experiments). **c** qRT-PCR analysis of LEE gene expression in WT and Δ*fusKR*, co-cultured with EcN3 in DMEM supplemented with GlcA and GOS or 2-FL ($n = 3$ independent experiments). **d** Adherence of WT and Δ*fusKR* to Caco-2 cells co-cultured with EcN3 in DMEM medium supplemented with GlcA and GOS or 2-FL ($n = 3$ independent experiments). **e** The survival of WT and Δ*fusKR* in Caco-2 cell culture supernatants co-cultured with EcN3 in DMEM medium supplemented with GlcA and GOS or 2-FL ($n = 3$ independent experiments). **f**, **g** FAS assay quantification of the number (**f**) and representative images (**g**) of pedestals per infected cell infected with WT and Δ*fusKR* co-cultured with EcN3, in DMEM medium supplemented with GlcA and GOS or 2-FL ($n = 50$ cells). The actin cytoskeleton (green) and nuclei of HeLa cells and bacteria (red) are shown. Arrowheads indicate the pedestals. Scale bar, 10 μm. Significance was determined by a two-tailed unpaired Student's *t*-test (**a**–**f**) and indicated as the *P* value. $^{*}P < 0.05$, $^{**}P < 0.01$, $^{***}P < 0.001$; ns no significant difference. Data were presented as mean ± s.d. (**b**–**f**). Source data are included in the Source Data file.

the mice infected with *C. rodentium* by analyzing the presence of mononuclear and polymorphonuclear infiltrates in the lamina propria, as well as alterations in mucosal architecture, villus height, goblet cell depletion, and the presence of attached bacteria. The histopathological scores for the EcN3/2-FL group were significantly lower than other groups observed in mice infected with *C. rodentium* (Fig. 4j, k), indicating that disease severity was reduced in the EcN3/2-FL group compared to other groups. Collectively, these data suggest that the administration of the combination of EcN3 and 2-FL can reduce the pathogenesis of *C. rodentium* during infection.

https://doi.org/10.1038/s41467-026-69126-4

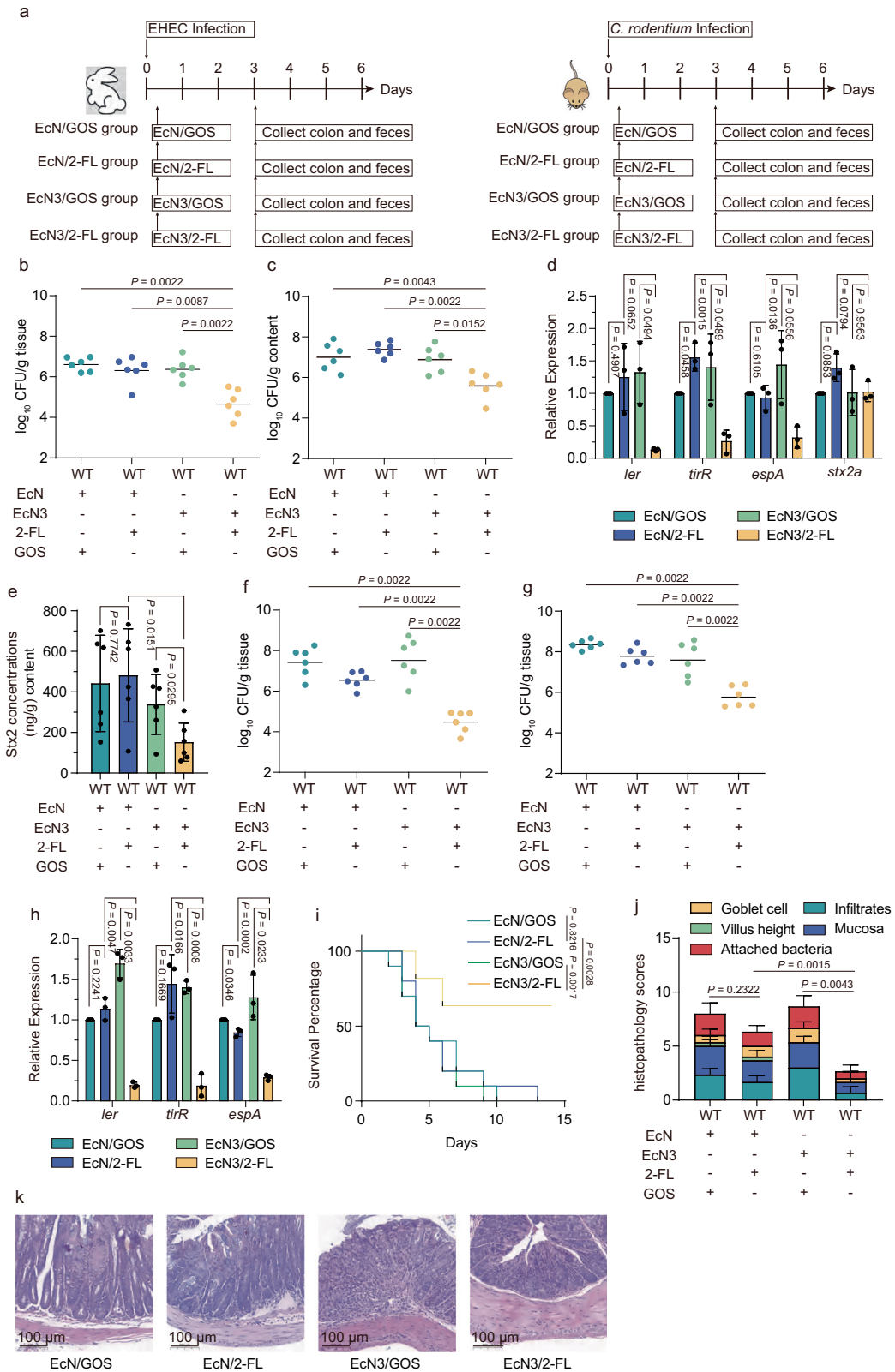

We further examined the preventive efficacy of the combination of EcN3 and 2-FL against *C. rodentium* infection (Supplementary Fig. 4a). The colonization assay showed that after administering the combination of EcN3 and 2-FL for 1–3 days before bacterial challenge, there was no significant decrease in colonization and survival compared to that in mice that did not receive any treatment (Supplementary Fig. 4b, c). Meanwhile, in vivo qRT-PCR analysis also presents comparable results, indicating that combining 2-FL and EcN3 does not effectively prevent *C. rodentium* infection (Supplementary Fig. 4d).

Further mice colonization experiments were performed to elucidate the mechanism underlying the preventive efficacy of the combination of EcN3 and 2-FL against *C. rodentium* infection. Following administration of the combination of EcN3 and 2-FL for 3 days, we separately administered equivalent therapeutic doses of EcN3 and 2-FL

Fig. 4 | The combination of EcN3 and 2-FL represses the pathogenesis of *C. rodentium*. **a** Schematic of EHEC and *C. rodentium* colonization in different infection models. **b**, **c** The intestinal tissue colonization ability (**b**) and luminal survival ability (**c**) of EHEC were determined in infant rabbits that were orally administered with 1×10^8 CFU EHEC followed by administration of 1×10^8 CFU EcN or EcN3 together with 2-FL or GOS ($n = 6$ mice per group). Horizontal bars indicate the median. **d** qRT-PCR analysis of virulence gene expression of EHEC in the colon obtained from rabbits administered with EcN or EcN3 and 2-FL or GOS ($n = 3$ independent experiments). **e** Stx2 concentrations (ng/g) in luminal contents of rabbits administered with EcN or EcN3 and 2-FL or GOS. The luminal contents were removed from the colon of rabbits 3 days post inoculation ($n = 6$ mice per group). **f**, **g** The intestinal epithelial colonization ability (**f**) and luminal survival ability (**g**) of *C. rodentium* in mice that were orally administered with 1×10^9 CFU *C. rodentium* followed by administration of 1×10^8 CFU EcN or EcN3 together with 2-FL or GOS ($n = 6$ mice per group). Horizontal bars indicate the median. **h** qRT-PCR analysis of LEE gene expression of *C. rodentium* in the colon obtained from mice administered with EcN or EcN3 and 2-FL or GOS ($n = 3$ independent experiments). **i** Survival curve of *C. rodentium*-infected mice following administrated with EcN or EcN3 and 2-FL or GOS ($n = 10$ mice per group). **j**, **k** Representative colon histology images (**j**) and histological score (**k**) of *C. rodentium*-infected mice following administrated with EcN or EcN3 and 2-FL or GOS ($n = 3$ independent experiments). Scale bar, 200 μm. Significance was determined by a two-sided Mann–Whitney *U*-test (**b**, **c**, **f**, **g**), log-rank (Mantel–Cox) test (**i**), or two-tailed unpaired Student's *t*-test (**d**,**e**, **h**, **j**) and indicated as the *P* value. $^*P < 0.05$, $^{**}P < 0.01$, $^{***}P < 0.001$; ns no significant difference. Data were presented as mean ± s.d. (**d**, **e**, **h**, **j**). Source data are included in the Source Data file.

during *C. rodentium* infection (EcN3 and 2-FL prevention group). Colonization assays revealed that administration of EcN3 showed no inhibitory effect, whereas administration of 2-FL significantly suppressed *C. rodentium* luminal content survival and intestinal tissue colonization capacity (Supplementary Fig. 4e, f). Further analysis of fecal samples collected after *C. rodentium* infection demonstrated comparable levels of EcN3 in EcN3 and 2-FL prevention groups (Supplementary Fig. 4g). These results suggest that although EcN3 can survive in the mice colon, 2-FL is metabolized by the gut microbiota due to their high metabolic activity, limiting its availability to exert protective effects against *C. rodentium* infection.

MCMs targeted the delivery of EcN3 and 2-FL to the colon separately

To enhance the preventive efficacy of the combination of EcN3 and 2-FL against *C. rodentium* infection, we performed MCMs, which are engineered to bypass the gastric environment and achieve precise delivery to the colon. The MCMs were prepared using gas-shearing, as illustrated in Fig. 5a. To validate the unique features of the MCMs, EcN was transformed with a fluorescent plasmid. At the same time, 2-FL was conjugated with FITC for fluorescence microscopy imaging, which was named E/H-MCMs. The fluorescence microscopy imaging and scanning electron microscope (SEM) results revealed distinct and non-overlapping distributions of the two fluorescent signals within the microcapsules, confirming the independence and stability of the dual-chamber structure (Fig. 5b, c and Supplementary Fig. 5a). This design effectively prevented EcN3 from prematurely utilizing 2-FL before reaching the target site, ensuring the functional integrity of both components. Furthermore, the particle size analysis confirmed that the size of the E/H-MCMs could be precisely controlled by adjusting the fabrication parameters (Supplementary Fig. 5b, c). The Young's modulus and stress-strain curve of E/H-MCMs were measured to assess their mechanical properties, indicating adequate structural stability for intestinal delivery (Supplementary Fig. 5d, e). Additionally, the cytocompatibility of the E/H-MCMs was evaluated using Live/Dead staining and a cell counting kit-8 (CCK-8) assay to assess their effects on the viability and proliferation of Caco-2 cells. The results showed that nearly all cells remained viable after a 7-day culture, indicating minimal cytotoxicity (Supplementary Fig. 5f). Furthermore, the CCK-8 assay showed no significant change in cell viability, demonstrating that the E/H-MCMs possess cytocompatibility (Supplementary Fig. 5g). The potential for diverse loading combinations of E/H-MCMs was also analyzed. The results of the loading combination potential in E/H-MCMs revealed that two distinct bacterial strains could be independently loaded into separate chambers of E/H-MCMs (Supplementary Fig. 3h), exhibiting broader application prospects and operational flexibility of diverse E/H-MCMs.

To analyze the degradation behavior of the microspheres, the E/H-MCMs were incubated in different simulated body fluids in vitro. It was observed that the morphology of E/H-MCMs remained unchanged in simulated gastric fluid (SGF). In contrast, they gradually dissolved after 4 hours of immersion in simulated colonic fluid (SCF) and were dissolved entirely by 24 h (Fig. 5d, e). Meanwhile, mice were administered E/H-MCMs via oral gavage, and imaging was performed using IVIS to quantify fluorescence intensity. The results indicated that E/H-MCMs reached the intestinal region and remained in vivo for up to 24 h (Fig. 5f, g). These findings confirmed that the E/H-MCMs effectively protected 2-FL and EcN from gastric degradation and enabled their accumulation in the colon.

To investigate the targeted delivery efficacy of E/H-MCMs in the colon, we orally administered either E/H-MCMs or an equivalent mixture of EcN3 and 2-FL for three consecutive days. After the 3-day administration, we observed a 14.04-fold reduction of EcN3 in the intestinal lumen of 2-FL-EcN3-treated mice compared with E/H-MCMs treated mice (Fig. 5h). Meanwhile, qRT-PCR results showed that the expression of the *uxaC*, *uxuB*, *uxuA*, and *fucA* in the colons of E/H-MCMs-treated mice were 8.89 to 13.88-fold higher than in 2-FL-EcN3-treated mice (Fig. 5i). In conclusion, these results demonstrate that E/H-MCMs effectively target the colon for the delivery and release of 2-FL and EcN3 in the colonic lumen.

E/H-MCMs offer prevention against *C. rodentium* infection

Previous results showed that E/H-MCMs can specifically release 2-FL and EcN3 in the colon. To evaluate the preventive efficacy of E/H-MCMs against EHEC and *C. rodentium* infection, we conducted infant rabbit and mouse colonization assays, respectively (Fig. 6a).

First, groups of infant rabbits were orally infected with 5×10^8 CFU EHEC O157:H7 and pretreated with the combination of EcN3 and 2-FL or E/H-MCMs for 1–3 days, respectively. Luminal survival and intestinal tissue colonization were assessed by quantifying bacterial loads in stool samples and on the colon. The results showed that E/H-MCMs administration significantly reduced both luminal survival and tissue colonization of EHEC in vivo (Fig. 6b, c). In vivo qRT-PCR further showed that LEE genes, but not stx2a, were significantly downregulated in the E/H-MCMs group (Fig. 6d). Consistently, measurements of Stx levels in vivo showed results similar to qRT-PCR, indicating that E/H-MCMs can be used to prevent EHEC infection (Fig. 6e).

We next tested the *C. rodentium* infection model. In EcN3/2-FL prevention group, the colonization capacity of *C. rodentium* was significantly higher than that in the luminal content and the colonic epithelium of E/H-MCMs prevention group indicating that E/H-MCMs significantly inhibited the *C. rodentium* colonization and survival ability in vivo (Fig. 6f, g). The qRT-PCR results also showed a 3.03 to 3.99-fold decrease of LEE gene expression in E/H-MCMs prevention group compared with infection and EcN3/2-FL prevention group (Fig. 6h). These results indicate that E/H-MCMs efficiently decrease the survival and colonization ability of *C. rodentium* in the colon of mice.

Next, we investigated the preventive efficacy of E/H-MCMs on the pathogenicity of *C. rodentium* by monitoring the lethality and

https://doi.org/10.1038/s41467-026-69126-4

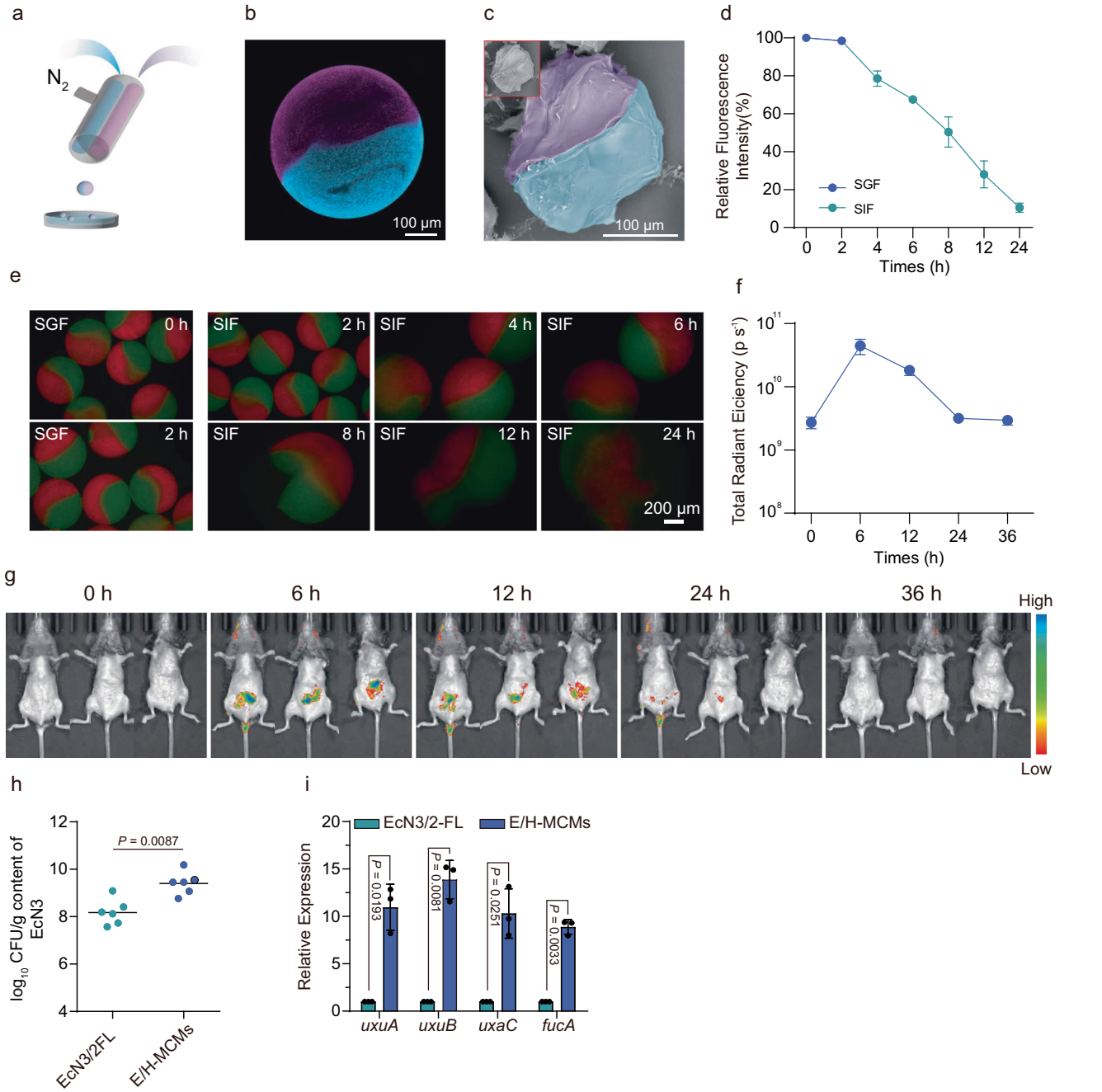

Fig. 5 | Development and characterization of E/H-MCMs for colon-targeted delivery. a Schematic illustration of MCMs fabrication using gas-shearing technology. **b**, **c** Representative fluorescence microscopy (**b**) and SEM (**c**) images showed distinct spatial separation of FITC-labeled 2-FL (blue) and EcN3 (violet) within dual-chamber microspheres ($n = 10$ microspheres). Scale bars, 100 μm. **d** Degradation profiles of E/H-MCMs in SGF and SCF ($n = 10$ independent experiments). Scale bars, 200 μm. **e** Representative image of E/H-MCMs degradation in SGF and SCF ($n = 10$ microspheres). Scale bars, 200 μm. **f** Quantification of fluorescence intensity of E/H-MCMs post-oral administration 36 h intestinal retention ($n = 3$ independent experiments). **g** Representative images of the gastrointestinal distribution of E/H-MCMs post-oral administration were shown ($n = 3$ mice per group). **h** Survival ability of EcN3 in mice administration EcN3 and 2-FL or E/H-MCMs ($n = 6$ mice per group). **i** qRT-PCR analysis of the expression of *uxaC*, *uxuB*, *uxuA*, and *fucA* of EcN3 survival in the colon of mice treated with EcN3/2-FL or E/H-MCMs ($n = 3$ independent experiments). Significance was determined by a two-sided Mann–Whitney *U*-test (**h**) or two-tailed unpaired Student's *t*-test (**i**) and indicated as the *P* value. $^{*}P < 0.05$, $^{**}P < 0.01$, $^{***}P < 0.001$; ns no significant difference. Data were presented as mean ± s.d. **i** Source data are included in the Source Data file.

histological damage in infected mice. The lethality curves of infected mice showed that E/H-MCMs prevention group presented decelerated mortality compared with infection and EcN3/2-FL prevention group (Fig. 6i). Histopathology scores in E/H-MCMs prevention group were significantly lower than those of infection and EcN3/2-FL prevention group (Fig. 6j, k), indicating the severity of disease caused by E/H-MCMs in mice was decreased compared to that caused by the combination of 2-FL and EcN3. These indicate that E/H-MCMs provide favorable outcomes in preventing *C. rodentium* infection.

E/H-MCMs restore *C. rodentium*-induced dysbiosis and intestinal barrier function

C. rodentium and EHEC infection have been shown to induce dysbiosis within the gut microbiota[32]. To assess whether treatment with E/H-

https://doi.org/10.1038/s41467-026-69126-4

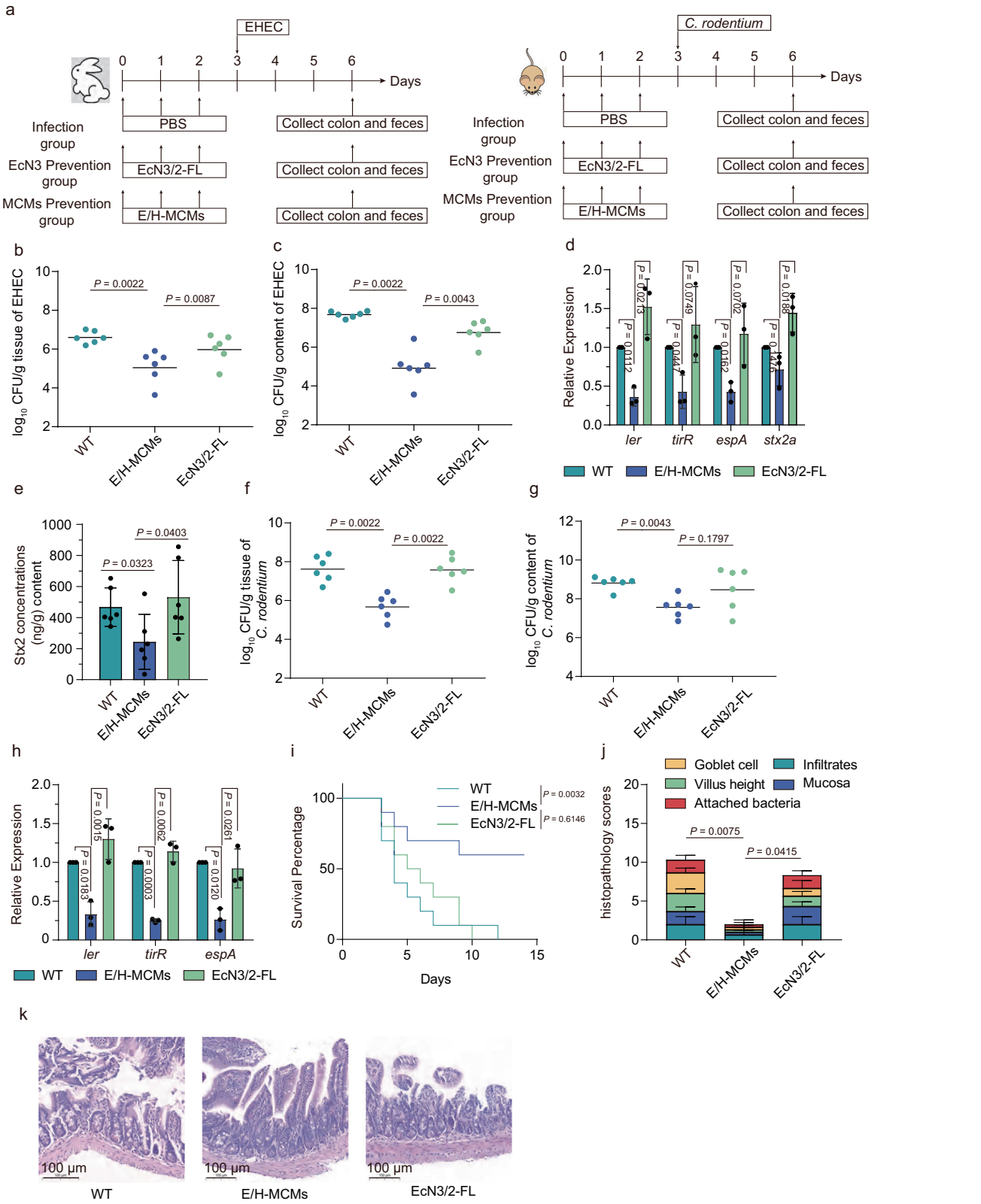

MCMs could restore the microbiome after infection, we conducted high-throughput sequencing analysis of the 16S rRNA gene in fecal bacterial DNA obtained from four groups of mice: uninfected group (UN), infection group, EcN/2-FL prevention group, EcN3/2-FL prevention group, MCMs prevention group, and E/H-MCMs prevention group.

Initially, we evaluated the alpha diversity of each group. The results revealed no significant differences in Shannon and ACE index in different groups (Fig. 7a, b). Additionally, we employed principal coordinate analysis (PCoA) using Bray-Curtis distance metrics and partial least squares discriminant analysis (PLS-DA) to assess the β-diversity of microbial communities among the groups. Notably,

Fig. 6 | E/H-MCMs prevention against *C. rodentium* colonization. a Schematic of EHEC and *C. rodentium* colonization in infant rabbit and mice prevention models. **b**, **c** The intestinal epithelial colonization ability (**b**) and luminal survival ability (**c**) of EHEC in infection, EcN3/2-FL prevention, and E/H-MCMs prevention groups ($n = 6$ mice per group). Horizontal bars indicate the median. **d** qRT-PCR analysis of virulence genes expression of EHEC in infant rabbit colon of infection, EcN3/2-FL prevention, and E/H-MCMs prevention groups ($n = 3$ independent experiments). **e** Stx2 concentrations (ng/g) in luminal contents of rabbits administrated with EHEC in infant rabbit colon of infection, EcN3/2-FL prevention, and E/H-MCMs prevention groups ($n = 6$ mice per group). The luminal contents were removed from the colon of rabbits 3 days post inoculation. **f**, **g** The intestinal epithelial colonization ability (**f**) and luminal survival ability (**g**) of *C. rodentium* in infection, EcN3/2-FL prevention, and E/H-MCMs prevention groups ($n = 6$ mice per group). Horizontal bars indicate the median. **h** qRT-PCR analysis of LEE genes expression of *C. rodentium* in the mice colon administration of infection, EcN3/2-FL prevention, and E/H-MCMs prevention groups ($n = 3$ independent experiments). **i** Survival curve of *C. rodentium*-infected mice in infection, EcN3/2-FL prevention, and E/H-MCMs prevention groups ($n = 10$ mice per group). **j**, **k** Histological score (**j**) and representative colon histology images (**k**) of mice in infection, EcN3/2-FL prevention, and E/H-MCMs prevention groups ($n = 3$ independent experiments). Scale bars: 100 μm. Significance was determined by a two-sided Mann–Whitney *U*-test (**b**, **c**, **f**, **g**), log-rank (Mantel–Cox) test (**i**), or two-tailed unpaired Student's *t*-test (**d**, **e**, **h**, **j**) and indicated as the *P* value. $^{*}P < 0.05$, $^{**}P < 0.01$, $^{***}P < 0.001$; ns no significant difference. Data were presented as mean ± s.d. (**d**, **e**, **h**, **j**). Source data are included in the Source Data file.

group-specific clustering was observed for the UN, infection group, EcN/2-FL prevention group, EcN3/2-FL prevention group, and MCMs prevention group (Fig. 7c, d). The E/H-MCMs prevention group clustered closely with the UN group in both PCoA and PLS-DA plots, indicating a microbial community structure more similar to uninfected controls (Fig. 7c, d). These findings confirmed that *C. rodentium* infection induces microbiota dysbiosis and demonstrate that E/H-MCMs treatment significantly modifies the intestinal bacterial community. Subsequently, the relative abundance of the gut microbiota was analyzed. At the genus level, the relative abundance of g_*Citrobacter* was significantly increased in the infection group and significantly decreased in the E/H-MCMs prevention group (Fig. 7e, f). In addition, the relative abundance of g_*Lactobacillus* and g_*Limosilactobacillus* was significantly increased in E/H-MCMs prevention group (Fig. 7e, g, h). At the family level, the relative abundance of f_*Enterobacteriaceae* group was significantly lower than that in E/H-MCMs prevention groups, and the relative abundances of f_*Lactobacillaceae* was significantly higher than those in UN and E/H-MCMs prevention groups (Supplementary Fig. 6a–c). Together, these results indicate that E/H-MCMs not only suppress pathogen growth (e.g., *Citrobacter*) but also promote the recovery and enrichment of beneficial commensals, thereby mitigating dysbiosis and supporting a healthier gut microbial community.

g_*Lactobacillus* and g_*Limosilactobacillus* belong to the family *Lactobacillaceae*, which is essential for maintaining a balanced and healthy intestinal environment and enhances intestinal barrier function[33]. We further confirmed whether E/H-MCMs treatment can promote the intestinal barrier function in vivo. The qRT-PCR results showed that the expression of *Muc-2* and *Zo-1* was significantly downregulated in the infection group, EcN/2-FL prevention group, EcN3/2-FL prevention group, and MCMs prevention group, and significantly upregulated in E/H-MCMs prevention group (Fig. 7i). In addition, mucin-specific Periodic Acid-Schiff (PAS) staining results showed that the mucus was more abundant in E/H-MCMs prevention group, indicating that E/H-MCMs can significantly promote the mucus secretion (Fig. 7j). The intestinal barrier integrity was assessed by permeability to 4 kDa fluorescein isothiocyanate (FITC)-dextran. It was observed that infection and EcN3/2-FL prevention groups markedly increased the serum FITC concentration compared with the UN group; however, the E/H-MCMs prevention group exhibited a serum FITC concentration that was comparable to that of the UN group (Fig. 7k), suggesting E/H-MCMs can recover the intestinal integrity destroyed by *C. rodentium* infection. These results demonstrated that E/H-MCMs lead to a notable increase in *Lactobacillaceae*, thereby protecting the intestinal barrier by promoting mucus secretion after *C. rodentium* infection.

Overall, these highlight the potential of MCMs in mitigating the adverse effects of EHEC infections and modulating the gut microbiota. These results suggest that MCMs could be a promising therapeutic and preventive strategy for managing EHEC infections and restoring microbial balance after pathogenic challenges.

Discussion

EHEC infections pose a significant global health challenge due to the potential for severe complications, such as HUS, and the limitations of current antibiotic treatments[3]. It is essential to develop therapeutic strategies that specifically target EHEC infections. In this study, we developed and validated a dual-mechanism therapeutic strategy against EHEC infection, simultaneously targeting metabolic competition and virulence gene silencing. Specifically, we engineered a probiotic strain, EcN3, which utilizes a 2-FL-responsive regulatory system to effectively compete with EHEC and *C. rodentium* for GlcA utilization, thereby restricting pathogen growth. Concurrently, the fucose released from 2-FL hydrolysis activates the FusKR two-component system, significantly suppressing the expression of virulence genes associated with the A/E lesion. Furthermore, we encapsulated EcN3 and 2-FL separately within MCMs, enabling targeted colonic delivery and protection from gastric degradation. This integrated approach effectively reduced pathogen colonization, virulence gene expression, and intestinal damage in vivo while preserving beneficial gut microbiota and mucosal integrity.

EHEC employs complex pathogenic mechanisms that enhance its pathogenicity in vivo. First, carbon sources are a limited resource in the gut, and their availability can prevent pathogen expansion[34,35]. EHEC has evolved specialized metabolic strategies to utilize alternative carbon sources, such as GlcA, GalA, and hexuronates, which are not preferred by commensal gut bacteria, thereby enhancing its colonization and pathogenicity[16,17]. Furthermore, EHEC senses various intestinal signals and coordinates the expression of virulence genes to initiate the disease-causing process[14,36]. Recognizing this, we demonstrated that EcN3 effectively outcompetes EHEC for GlcA, significantly reducing pathogen growth. Although GlcA is a common carbon source for multiple gut bacteria, including probiotics and pathogens such as EcN, *C. rodentium*, and *Bacteroides fragilis*, which makes simple GlcA depletion an apparently non-selective strategy. Our approach achieves inhibition of EHEC through a combination of targeted delivery, localized GlcA competition, and virulence attenuation rather than broad-spectrum depletion. While GlcA depletion alone may not be specific, our design couples local carbon competition with 2-FL/fucose signaling, which downregulates LEE gene expression and colonization capacity, thereby reducing EHEC colonization and toxicity. In future research, we plan to further modulate EcN3's metabolic control and the delivery system so that high-level GlcA consumption is activated only under EHEC-enriched conditions (e.g., at infection peaks and localized sites), further minimizing the impacts on commensals.

Recent studies have also highlighted the therapeutic potential of 2-FL in various infectious diseases, including *Clostridioides* difficile and EAEC infections, supporting our choice of 2-FL for developing an effective therapeutic approach[35,37]. EcN has been utilized to treat multiple diseases, such as infectious diseases, metabolic disorders, and inflammatory bowel diseases[28]. Meanwhile, EcN is a non-colonizing, well-established probiotic strain, providing a flexible platform for developing engineered bacterial therapeutics[38]. Based on these

https://doi.org/10.1038/s41467-026-69126-4

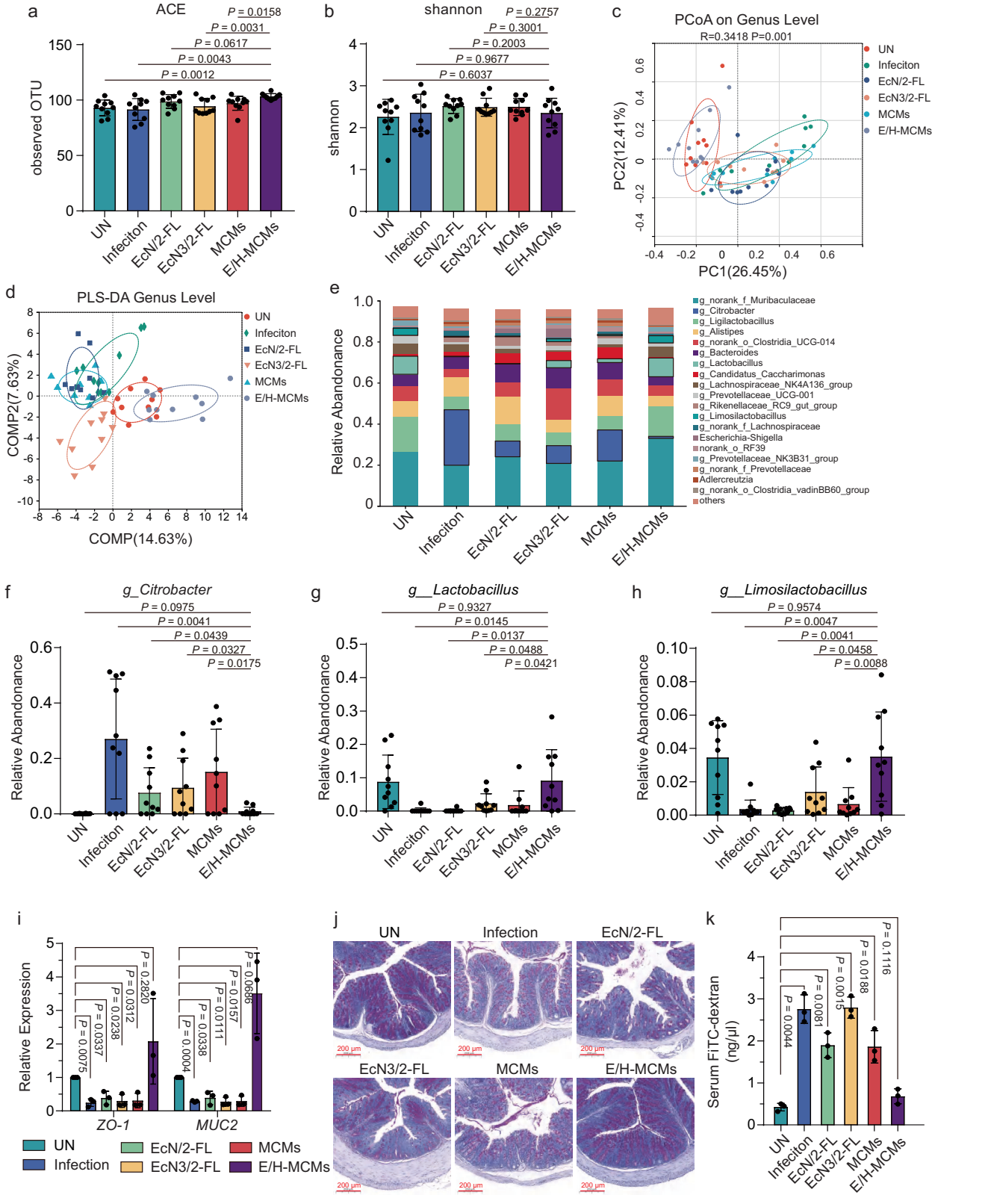

characteristics, we developed a dual-layer regulatory system incorporating 2′-fucosyllactose (2′-FL) as an exogenous signaling molecule, which also demonstrated higher efficiency in resource utilization and gene regulation. In this system, *fucA* is driven by the PfnrS promoter and expressed exclusively under anaerobic conditions, enabling hydrolysis of 2′-FL to generate lactose and fucose. Lactose functions as a secondary signal to induce the lactose-responsive promoter, thereby driving the expression of GlcA catabolic genes and GlcA utilization. Fucose has been shown to significantly repress virulence gene expression in A/E pathogens such as *C. rodentium*[15,39]. Furthermore, 2′-FL itself, as a prebiotic, promotes the growth of commensal bacteria such as *Lactobacillus*, improving gut microbiota composition and further enhancing overall therapeutic potential. So, ECN3 activated the target pathway only in the presence of 2′-FL, which significantly

Fig. 7 | H/E-MCMs restore gut microbiota and combat *C. rodentium*-induced dysbiosis. a, **b** ACE richness estimator (**a**) and Shannon diversity index (**b**) of fecal microbiota in uninfected (UN), infection, EcN3/2-FL prevention, and E/H-MCMs prevention groups ($n = 10$ mice per group). **c**, **d** Beta diversity analysis of fecal microbiota assessed by PCoA (**c**) and PLS-DA (**d**) for the UN, infection, EcN/2-FL prevention, EcN3/2-FL prevention, MCMs, and E/H-MCMs prevention groups ($n = 10$ mice per group). **e** Relative abundance of fecal gut microbiota at the genus level in UN, infection, EcN/2-FL prevention, EcN3/2-FL prevention, MCMs, and E/H-MCMs prevention groups ($n = 10$ mice per group). **f**–**h** Relative abundance of g_*Citrobacter*(f), g_*Lactobacillus* (**g**), g_*Limosilactobacillus* (**h**) in the colon of UN, infection, EcN/2-FL prevention, EcN3/2-FL prevention, MCMs, and E/H-MCMs prevention groups ($n = 10$ mice per group). **i** qRT-PCR analysis of the expression of *Zo-1* and *Muc-2* in the colonic epithelium of UN, infection, EcN/2-FL prevention, EcN3/2-FL prevention, MCMs, and E/H-MCMs prevention groups ($n = 3$ independent experiments). **j** Representative PAS staining images of the colonic mucus layer of UN, infection, EcN/2-FL prevention, EcN3/2-FL prevention, MCMs, and E/H-MCMs prevention groups ($n = 3$ independent experiments). Scale bars: 100 μm. **k** FITC-dextran levels in serum of UN, infection, EcN/2-FL prevention, EcN3/2-FL prevention, MCMs, and E/H-MCMs prevention groups as a measure of intestinal permeability ($n = 3$ independent experiments). Significance was determined by a two-tailed unpaired Student's *t*-test (**a**, **b**, **f**, **g**, **h**, **i**, **k**) and indicated as the *P* value. $^{*}P < 0.05$, $^{**}P < 0.01$, $^{***}P < 0.001$; ns no significant difference. Data were presented as mean ± s.d. (**a**, **b**, **f**–**i**, **k**). Source data are included in the Source Data file.

reduced energy expenditure. When needed, supplementation with 2′-FL rapidly initiated GlcA metabolism and antibacterial functions, thereby enabling "on-demand activation" and dynamic control. Moreover, this design exhibits strong modularity and engineering flexibility. By decoupling the environmental sensing module from the metabolic function module, the lactose-responsive element can be readily substituted with other signal-responsive elements, enabling rapid adaptation to different hosts or infection scenarios and broadening the scope of application. Therefore, combining 2-FL and EcN3 represents a safe and efficient strategy for treating EHEC infections. This combinational approach provides a comprehensive strategy simultaneously targeting pathogen metabolism and virulence.

Despite the promising therapeutic efficacy demonstrated by EcN3 and 2-FL, our initial findings indicated the limitations of the combination of EcN3 and 2-FL in preventive capability against EHEC infection. Previous studies have shown that 2-FL is readily metabolized by microbiota, promoting the abundance of beneficial microbes, such as *Bifidobacteria* and *Lactobacillus*[40]. However, the metabolic capacity of microbiota limited its sustained therapeutic action availability. To overcome this limitation, we developed E/H-MCMs constructed from sodium alginate, which exhibits pH-responsive properties. These E/H-MCMs effectively protect encapsulated probiotics and small molecules from gastric degradation, ensuring targeted and sustained release in the colon. E/H-MCMs-mediated delivery significantly increases colonic concentrations of 2-FL, as well as the bacterial load of EcN3, thereby enhancing preventive efficacy against *C. rodentium* infection. Additionally, the versatility of MCMs in simultaneously encapsulating diverse bacterial strains and small molecules without cross-interference opens avenues for developing therapeutic strategies targeting different pathogens and diseases.

Conventional antibiotics are contraindicated in EHEC infections due to the risk of toxin release and disruption of gut microbiota[41]. In contrast, our approach targets pathogen metabolism and virulence regulation, minimizing adverse effects on commensal bacteria. Furthermore, E/H-MCMs contributed to the re-establishment of intestinal microbiota disrupted by pathogenic infections, significantly enhancing the relative abundance of *Lactobacillus*, a genus essential for maintaining gut barrier integrity and facilitating mucus secretion[42]. This effect may be attributed to 2-FL, a member of a diverse group of non-digestible complex carbohydrates, which is important in the development and maintenance of healthy gut microbiota, thereby promoting the proliferation and adherence capacity of *Bifidobacteria* and *Lactobacillus*[43–45]. Additionally, *Lactobacillus* is capable of metabolizing fucose within the intestine, resulting in the production of metabolites such as short-chain fatty acids (SCFAs) and 1,2-propanediol (1,2-PDO), which have been documented to confer various health benefits[46,47]. Moreover, 2-FL can directly modulate intestinal goblet cells to enhance mucus barrier function[48]. These suggest that E/H-MCMs not only inhibit EHEC infection through multiple mechanisms but also promote the rapid recovery of the damaged intestine, thereby expediting the disease recovery process. By employing a probiotic-based system rather than broad-spectrum antibiotics, our strategy provides a promising alternative to address the global challenge of antibiotic resistance.

In conclusion, our study demonstrates that the EcN3/2-FL combination delivered via MCMs represents an effective therapeutic strategy against EHEC infections. This approach significantly reduces pathogen colonization and intestinal damage while preserving beneficial gut microbiota by precisely modulating pathogen nutrient availability and virulence gene expression. Future research should focus on evaluating the long-term safety profile, optimizing MCM manufacturing processes, and conducting rigorous clinical evaluations. Ultimately, this dual-mechanism strategy holds significant promise for managing enteric infections and addressing the growing global threat of antibiotic resistance.

Methods

Bacterial strain and plasmid construction

The bacterial strains and plasmids used in this study are provided in Supplementary Data 1 and 2. For EcN1 construction, the *uxaC*, *uxuB*, and *uxuA* genes were PCR amplified from EHEC and ligated into a pACYC vector under the control of a constitutive promoter using the SPARKeasy Gel DNA Extraction Kit (Sparkjade, AE0101) and then transferred into EcN. For EcN2 construction, a lactose-inducible promoter was used to replace the constitutive promoter of pACYC. For EcN3 stain construction, genes encoding α-L-fucosidase from Thermotoga maritima with PfnrS promoter were cloned into the pACYC plasmids. Mutant strains were generated using the λ-Red recombination system. Bacterial strains were generally cultured in LB medium under aerobic conditions at 37 °C. Isopropyl β-D-thiogalactoside (IPTG) and antibiotics were supplemented in the medium when required using the following final concentrations: 0.1 mM IPTG, ampicillin (100 μg/mL); nalidixic acid (25 μg/mL); chloramphenicol (50 μg/mL); kanamycin (50 μg/mL); erythromycin (500 μg/mL).

Growth assay

To determine the growth curve of EcN and EcN1, overnight cultures were diluted 1:100 in a flask containing 20 mL of M9 medium containing 6 g/L GlcA as the sole carbon source. To determine the growth curve of EcN and EcN2, overnight cultures were diluted 1:100 in a flask containing 20 mL of M9 medium containing 6 g/L GlcA and 0.1 mM IPTG. To determine the growth curve of EcN and EcN3, overnight cultures were diluted 1:100 in a flask containing 20 mL of M9 medium containing 6 g/L GlcA and 2 g/L 2-FL (catalog #GY1141M, HuicH, Shanghai, China) as the sole carbon source. Next, a 200 μL aliquot was added to a 96-well microplate and incubated at 37 °C with shaking at 180 rpm for 24 h. The absorbance at 600 nm was recorded every 30 min. Experiments were independently performed three times.

For competitive growth assays, 10^5 CFU of EcN and WT or 10^5 CFU of EcN3 and WT were co-cultured in M9 medium supplemented with either GlcA and GOS or 2-FL. After 8 h of incubation, a 100 μL aliquot was removed, and suitable dilutions were plated onto LB agar plates containing antibiotics. The competitive index (CI) values were

calculated as the ratio of the number of EcN/WT or EcN3/WT. Experiments were independently performed three times.

Concentration detection of 2-FL and GlcA in vitro

To quantify GlcA and 2-FL concentrations in vitro, 500 µL of the bacterial culture was collected and centrifuged at 4000×*g* for 5 min at 4 °C. The supernatant was then filtered through a 0.22-µm filter to remove any microbial contamination, and the filtered sample was analyzed using high-performance liquid chromatography (HPLC). The HPLC analysis was performed on an UltiMate 3000 HPLC system (Thermo Scientific, USA) with an ROA-Organic Acid H^+ column (300 × 7.8 mm). Detection was done using a UV detector at 210 nm and a refractive index detector (RefractoMax 521, Thermo Scientific, USA). The mobile phase consisted of 10 mM H_2SO_4, with a 0.5 mL/min flow rate.

UHPLC-MS/MS analysis

To quantify in vivo glucuronic acid (GlcA) concentrations, six biological replicates are included per group. For each replicate, 50 mg of fecal material is weighed and extracted with 500 µL of 80% (v/v) aqueous methanol. The mixture was ground for 6 min (−10 °C, 50 Hz), followed by cryogenic ultrasonic treatment for 10 min (5 °C, 40 KHz). After centrifugation at 14,000×*g* for 15 min at 4 °C, 300 µL of the supernatant was aliquoted. Then, 15 µL of internal standard mixture was added, and the mixture was vortexed before direct injection for analysis. An additional 300 µL of supernatant was dried under nitrogen and then reconstituted with 75 µL of 50% acetonitrile aqueous solution (containing 20% internal standard mixed reserve solution). The supernatant was injected into the LC-MS/MS system for analysis.

All samples were analyzed at Majorbio Bio-Pharm Technology Co., Ltd. (Shanghai, China) using an ExionLC AD system equipped with a BEH HILIC column (4.6 × 250 mm,5 µm). The injection volume was 5 µL, and the column temperature was maintained at 40 °C. The mobile phases consisted of solvent A (15 mM NH_4HCO_3 and 0.4% aqueous ammonia) and solvent B (acetonitrile), with a total chromatographic run time of 22 min. The gradient elution program was as follows: 0–2 min, 60% A (flow rate: 0.30 mL/min); 2–6 min, 60–95% A (flow rate: 0.30 mL/min); 6–9 min, 95–90% A (flow rate: 0.30 mL/min to 0.35 mL/min); 9–12 min, 90–95% A (flow rate: 0.35 mL/min); 12–15 min, 95% A (flow rate: 0.35 mL/min to 0.60 mL/min); 15–17 min, 95–60% A (flow rate: 0.60 mL/min); and 17–20 min, 60% A (flow rate: 0.60 mL/min to 0.30 mL/min). The column was subsequently re-equilibrated for 2 min prior to the next injection.

Data acquisition was performed using a UHPLC system connected to a QTRAP® 7500+ mass spectrometer (Sciex, USA) equipped with an electrospray ionization (ESI) source operating in negative mode. The parameters were set as follows: source temperature, 550°C; curtain gas (CUR), 40 psi; collision-activated dissociation (CAD) gas pressure, medium; ion source gas 1 and gas 2, 60 psi each; ion-spray voltage floating (ISVF), -4500 V. Data were acquired in multiple reaction monitoring (MRM) mode. During instrumental analysis, one quality control (QC) sample was injected after every five samples to monitor analytical reproducibility, and the relative standard deviation (RSD) of the target metabolite was required to be less than 15%.

LC-MS raw data were imported into Sciex OS software (version 3.x; AB SCIEX, Framingham, MA, USA). All ion fragments were automatically identified and integrated using default parameters, and all integrations were manually verified. The metabolite concentrations of the samples were calculated based on a linear regression standard curve. The concentration data matrix was uploaded to the Majorbio Cloud Platform (cloud.majorbio.com) for statistical analysis. Statistically significant differences in metabolite concentrations were identified using Student's *t*-test with a significance threshold of $p < 0.05$.

RNA isolation and qRT-PCR assay

Overnight culture was 1:100 subcultured in 20 ml fresh DMEM medium supplemented with 6 g/L GlcA and 2 g/L GOS or 2 g/L 2-FL at 37 °C with shaking at 180 rpm until the exponential growth phase was reached (OD_{600} = 0.6–0.8). The mice colon was harvested. Total RNA was extracted with TRIzol Reagent (Invitrogen; 5596026). DNase digestion was done on-column using an RNase-free DNase set (Qiagen; 79254) to remove possible DNA contamination. The integrity and purity of RNA were quantified by gel electrophoresis, and absorbance was measured using a Nanodrop 2000. For qRT-PCR analysis, total RNA was reverse transcribed using the StarScript III RT MasterMix (Genestar, A233) to synthesize the cDNA. cDNA was used as a template, mixed with a SYBR Green fluorescence dye (Genestar, A304) and added with forward and reverse primers (Supplementary Data 3). qRT-PCR was performed in an ABI 7500 thermocycler with sequence detection. The level of *uxaC*, *uxaB*, *uxaA*, *fucA*, and LEE genes was normalized according to the *rpoA* expression[49] and the level of *Zo-1* and *Muc-2* genes was normalized according to the *Gapdh* expression. Fold changes in gene expression were calculated using the $2^{-\Delta\Delta Ct}$ method. Data were collected from at least three biological replicates.

Cell adherence assay

HeLa and Caco-2 cells were purchased from the Shanghai Institute of Biochemistry and Cell Biology of the Chinese Academy of Science (SCSP-504 and SCSP-5027) and cultured in DMEM supplemented with 10% fetal bovine serum (FBS) at 37 °C in a 5% CO_2 incubator.

HeLa and Caco-2 cells were seeded into six-well plates with DMEM containing 10% FBS overnight. The bacterial cultures were incubated overnight at 37 °C and then subcultured in DMEM at 37 °C until reaching an OD_{600nm} of 0.6. The bacteria were eventually collected by centrifugation. After washing with PBS and resuspending in fresh DMEM, supplemented with 6 g/L GlcA and 2 g/L GOS or 2 g/L 2-FL, logarithmic bacterial cultures were used to infect confluent monolayers of HeLa or Caco-2 cells for 3 h at 37 °C and 5% CO_2 with a multiplicity of infection (MOI) of 100. After incubation for 3 h, the supernatant was diluted and plated on LB agar, and the cells were washed with PBS six times and lysed with 0.1% Triton X-100 for 5 min. The lysate was diluted and plated on LB agar. The attachment efficiency was determined by counting the CFU per milliliter. Each experiment was carried out three times.

Fluorescent actin staining (FAS)

HeLa cells were cultured on coverslips in 6-well plates and subsequently infected with bacteria. After 3 h of infection, the coverslips were washed with PBS, fixed with 4% paraformaldehyde, and permeabilized with 0.01% Triton X-100. Subsequently, the cells were treated with fluorescein isothiocyanate (FITC)-labeled phalloidin (Sigma-Aldrich, #P5282) to visualize actin accumulation and with propidium iodide (Sigma-Aldrich, #P4864) to visualize host cell nuclei and bacteria. The coverslips were mounted on slides and imaged using a Zeiss LSM 800 microscope (Zeiss, Germany). The percentage of infected cells and the number of pedestals per infected cell were counted from 50 cells on five slides.

C. rodentium colonization and survival assay

Five- to six-week-old female SPF C57B6/J mice were purchased from Beijing Vital River Laboratory Animal Technology (Beijing, China). All mice were housed in a temperature-controlled room with a 12-h light/12-h dark cycle, a temperature of 22 ± 2 °C, and a relative humidity of 50–60%. Animals had free access to autoclaved drinking water and a standard rodent chow (SPF-F02-002), which contains ~18% crude protein, 5% crude fat, and 5% crude fiber.

Bacteria were grown overnight in LB broth supplemented with the corresponding antibiotics. Mice were infected by oral gavage with

100 μL of PBS containing ~1×10^9 CFU of *C. rodentium*. Three days after infection, the mice were sacrificed. The colons and luminal content were aseptically removed and homogenized in sterile PBS. The bacterial CFUs were counted by spreading the bacterial suspensions on the surfaces of agar plates containing the corresponding antibiotics. Colony counts from the colon tissue were used to quantify intestinal tissue colonization ability, whereas counts from the luminal contents were used to quantify luminal survival ability.

To treat *C. rodentium* infection, mice were orally infected with 10^9 CFU of *C. rodentium*, 2 h later, received an oral dose of 1×10^8 CFU EcN3 (or EcN) together with 20 mg GOS (or 2-FL). To prevent *C. rodentium* infection, mice were pretreated with 0.5% E/H-MCMs or 1×10^8 CFU EcN3 and 20 mg 2-FL orally administered for three consecutive days before the *C. rodentium* challenge. For the survival assay, mice were pretreated with E/H-MCMs or EcN3/2-FL for 3 days before *C. rodentium* challenge, or mice were orally infected with 10^9 CFU of *C. rodentium*, followed by administration of 1×10^8 CFU EcN3 (or EcN) and 20 mg GOS (or 2-FL). Survival was monitored daily at consistent time points throughout the study.

Infant rabbit colonization model of EHEC

Female New Zealand white rabbits (3-day-old) were housed in a temperature-controlled room with a 12-h light/12-h dark cycle, a temperature of 22 ± 2 °C, and a relative humidity of 50–60%. The infant rabbits were maintained with the dam and nursed ad libitum. Infant rabbits were orally inoculated with EHEC O157:H7 strain EDL933 to establish intestinal colonization[50]. In the therapeutic model, animals were first infected with 5×10^8 CFU EDL933 and subsequently received post-infection intervention with 1×10^8 CFU EcN3 together with 2-FL. In the prevention model, infant rabbits were pretreated for 1–3 consecutive days with either 1×10^8 CFU EcN3 with 2-FL or E/H-MCMs prior to EDL933 challenge. At the indicated endpoints, luminal contents and colon tissues were collected aseptically. Bacterial burdens were quantified as CFU per gram from luminal contents (luminal survival) and colon tissue homogenates (tissue colonization). Virulence gene expression (LEE genes and *stx2a*) in colon tissue was measured by qRT-PCR, and total luminal Stx2 levels were determined by ELISA.

Stx detection by ELISA

The secretion of Stx2 was detected using an ELISA kit (Shanghai Yuanxin Bio Co., Ltd, YX155149). Supernatants from infected cells and homogenates of infected ileal tissues were analyzed following the manufacturer's ELISA protocol. After the ELISA procedure, the optical density (OD) of the samples at 450 nm was measured using a Spark 10 M multimode microplate reader (Tecan)[51].

Histological analysis

Five- to six-week-old female C57B6/J mice were infected by oral gavage of 10^9 CFU of *C. rodentium* in 100 μL PBS following treatment with EcN3/2-FL or MCMs. After 3 days, the distal colon was harvested. The colon samples were fixed in 10% neutral buffered formalin overnight and embedded in paraffin. The paraffin-embedded sections were deparaffinized and stained with hematoxylin-eosin, and the stained sections were blindly scored for inflammation severity. In brief, the severity of inflammation was assessed based on the following histopathological features: the intensity of infiltrates in the lamina propria, the changes in the architecture of the mucosa, the villus height, goblet cell depletion, and attached bacteria. The changes were graded for each parameter according to the following scale: 0, absent; 1, mild; 2, moderate; and 3, intense.

Fabrication of MCMs

The gas-shearing microfluidic platform mainly consists of four parts: an electronic syringe pump for providing alginate solution; a nitrogen cylinder supplying nitrogen gas, regulated by a flowmeter to control the nitrogen flow rate; a custom-made dual channel coaxial needle system, with two inner 30 G needles inserted in an outer needle for transporting liquids and an 18G needle inserted in the outer needle for transporting nitrogen gas; and a collection bath containing $CaCl_2$ solution.

For the fabrication of the MCMs, 2% (w/v) 2-FL or 1×10^{10} CFU/ml EcN(GPF labeled), EcN3 or *Lactobacillus murinus* (mCherry labeled) were mixed with 1% (w/v) alginate and pumped into the different liquid transporting channels, respectively. The flow rate of alginate was set at 3 ml/h. Nitrogen gas was transported into the outer needle to provide a shearing force for the formation of microdroplets. The flow rate of nitrogen gas was 3 L/min. Then, 2% (w/v) $CaCl_2$ was used in the collection bath to crosslink the alginate.

The morphology of MCMs

Multiple imaging techniques were employed to evaluate the morphology and structural characteristics of the microgels. Optical and fluorescence images of the MCMs were first acquired using a fluorescence microscope (MSHOT MF53-N) to provide an overview of the size distribution and preliminary structural features. Laser scanning confocal microscopy (ELYPA, P.1, Zeiss) was performed for higher-resolution fluorescence imaging. The diameters of MCMs were quantitatively analyzed using ImageJ software. At least 100 individual microgels were measured for statistical reliability. SEM was performed to investigate the microgels' surface morphology and microstructural details in the dry state. The microgels were freeze-dried using a lyophilizer, then mounted onto aluminum stubs with double-sided carbon tape, and sputter-coated with a thin layer of gold or platinum using a sputter coater to enhance conductivity. SEM imaging was carried out using a benchtop scanning electron microscope (TM4000plus).

Mechanical testing of MCMs

Compression tests were performed on a monolayer of MCMs to evaluate the bulk mechanical properties of MCMs. MCMs with a uniform diameter of ~400 μm were fabricated using a gas-shearing microfluidic platform. Following preparation, microgels were washed with PBS and maintained hydrated throughout the testing process to preserve their native mechanical properties. For testing, a single layer of MCMs was evenly spread and arranged on the flat platform of a Texture Analyzer (TA.XT PlusC, Stable Micro Systems, UK). A flat-ended cylindrical stainless-steel probe was used to apply compressive force uniformly across the microgel layer. Compression was carried out at a constant speed of 0.01 mm/s; the force-displacement data were recorded in real-time.

In vitro biocompatibility analysis of MCMs

The cell counting kit-8 (CCK-8) assay was employed to assess cell proliferation in hydrogel materials. MCMs were incubated in DMEM for 1, 4, and 7 days to obtain leaching solutions. Caco-2 cells were seeded in a 96-well plate at 10,000 cells/well density, cultured with the leaching solution for 1, 4, and 7 days, and subjected to CCK-8 incubation at 37 °C for 40–90 min. Absorbance was measured at 450 nm using a microplate reader.

To evaluate the toxicity of MCMs, samples were placed on round glass slides at the bottom of a 12-well plate, and Caco-2 cells were seeded in the plate. Live/dead staining was performed on days 1, 4, and 7 using the Calcein-AM/PI kit (servicebio, G1707). Images were captured using fluorescence microscopy (ZEISS, Germany) with excitation at 488 and 568 nm; green fluorescence indicated live cells and red fluorescence indicated dead cells, allowing for cell number and viability assessment. All experiments were performed independently in triplicate.

In vitro dissolution experiment of MCMs

MCMs were immersed in simulated gastric fluid (Coolaber, SL6600A) for 2 h and then transferred to simulated colonic fluid (Coolaber, SL66101). The dissolution of MCMs was observed under a microscope at regular intervals, and fluorescence intensity was quantified using ImageJ.

Bioluminescence imaging

Bioluminescence imaging (BLI) technology was performed using an IVIS Spectrum (PerkinElmer) imaging scanner coupled with Living Image Software (PerkinElmer). Briefly, at different time points, 100 μL of 0.5% fluorescent E/H-MCMs were administered via oral gavage to each mouse. Before scanning, the abdominal cavity of mice was shaved to allow accurate collection of fluorescent signals. Images were collected at regular intervals after gavage using the IVIS Imaging System (PerkinElmer IVIS Lumina LT), and fluorescence intensity in the digestive tract was quantified using Living Image Software.

16S rRNA sequencing and analysis

Metagenomic DNA was extracted from fecal samples using a FastPure Feces DNA Isolation Kit (MJYH, Shanghai, China), and its quality was assessed. The V3-V4 region of the bacterial 16S rRNA was amplified using specific primers 338F and 806R. The PCR amplification products were purified using the AxyPrep DNA Gel Extraction Kit (Axygen, Shanghai, China) and subjected to high-throughput sequencing on the Illumina MiSeq platform using the Nexseq 2000 (Illumina, California, USA). The resulting high-quality sequences were flattened according to the minimum sample sequence number. Subsequently, the sample operational taxonomic units (OTUs) were annotated and evaluated for species identification. To obtain species classification information for each OTU, the Bayesian algorithm of the RDP classifier was employed to analyze the OTU sequences with 97% similarity at various taxonomic levels.

Periodic acid-Schiff (PAS) staining

First, the colon samples were collected and fixed. After dehydrating the paraffin sections, the slices were oxidized in a 1.0% periodic acid solution for 10 min and then washed in distilled water for 5 min. The sections were stained with Schiff's solution for 30 min in the dark and washed again for 5 min. Once dried, the nuclei were lightly stained with Mayer's hematoxylin for ~1 min, rinsed in running water for several minutes, dehydrated in a gradient of alcohol, cleared with xylene, and finally mounted with neutral gum.

In vivo gut permeability assay

At 7 d postinfection, mice were deprived of food overnight and administered a FITC-conjugated dextran probe by orgastric gavage (molecular weight 3000–5000 kDa; 600 mg/kg), and blood was collected after 4 h by cardiac puncture. Serum was collected and separated by centrifugation at 12,000×*g* for 10 min, at 4 °C and 200 μL of each sample was added to a 96-well black microplate. Fluorescence was read at 485/528 nm wavelength. All experiments were performed independently in triplicate[52].

Statistics and reproducibility

No statistical methods were used to predetermine sample sizes, but our sample sizes are similar to those reported in previous publications[50,53]. Animals were randomly assigned to control and manipulation groups and data collection. Experimenters were unaware of the experimental conditions of the animals at the time of testing. Other data collection was not randomized but was always done in parallel with controls. No exclusions of animals or data points were reported. Most experiments were conducted by at least two researchers who did not know the situation and results of the study in advance, and repeated on at least two independent days.

Student's unpaired *t*-test performed statistical analyses. The Mann–Whitney test was used for all mouse colonization experiments to determine the statistical significance. The survival analysis statistics were calculated using the log-rank (Mantel–Cox) test. Detailed information on the number of biological samples and animals used can be found in the figure legends. Data distribution was assumed normal, but this was not formally tested. All statistical analyses were performed using GraphPad Prism 7 software.

Ethics statement

All animal experiments were performed according to protocols approved by the Institutional Animal Care and Use Committee of Nankai University (Tianjin, China). Experiments involving five- to six-week-old female C57BL/6J mice are conducted under protocol No. 2020030501, and experiments involving 3-day-old female New Zealand white infant rabbits are conducted under protocol No. SYDWLL-000165. All procedures comply with the standards set forth in the Guide for the Care and Use of Laboratory Animals.

Reporting summary

Further information on research design is available in the Nature Portfolio Reporting Summary linked to this article.

Data availability

The raw sequencing data of 16S rRNA gene sequencing in this study have been deposited in the Genome Sequence Archive (GSA) at the BIG Data Center, Beijing Institute of Genomics, Chinese Academy of Sciences, under accession code CRA024889. The metabolomic data have been uploaded into the Open Archive for Miscellaneous Data under accession Number: OMIX013933. The relevant experimental data and metadata generated in this study are provided in the manuscript, Supplementary Information, and Source Data file. Source data are provided with this paper.

References

1. Mancuso, G., Midiri, A., Gerace, E. & Biondo, C. Bacterial antibiotic resistance: the most critical pathogens. *Pathogens*. **10**, 1310 (2021).
2. Liu, Y. et al. LysR-type transcriptional regulator OvrB encoded in O island 9 drives enterohemorrhagic *Escherichia coli* O157:H7 virulence. *Virulence* **10**, 783–792 (2019).
3. Feitz, W. J. C. et al. Primary human derived blood outgrowth endothelial cells: an appropriate *in vitro* model to study Shiga toxin mediated damage of endothelial cells. *Toxins* **12**, 483 (2020).
4. Mühlen, S. et al. Identification of antibiotics that diminish disease in a murine model of enterohemorrhagic *Escherichia coli* infection. *Antimicrob. Agents Chemother.* **64**, e02159-19 (2020).
5. Shi, Y. et al. Structural and functional alterations in the microbial community and immunological consequences in a mouse model of antibiotic-induced dysbiosis. *Front. Microbiol.* **9**, 1948 (2018).
6. Sun, H. et al. Key roles of two-component systems in intestinal signal sensing and virulence regulation in enterohemorrhagic *Escherichia coli*. *FEMS Microbiol. Rev.* **48**, fuae028 (2024).
7. Gelalcha, B. D., Brown, S. M., Crocker, H. E., Agga, G. E. & Kerro Dego, O. Regulation mechanisms of virulence genes in enterohemorrhagic *Escherichia coli*. *Foodborne Pathog. Dis.* **19**, 598–612 (2022).
8. Vlisidou, I. et al. Role of intimin-tir interactions and the tir-cytoskeleton coupling protein in the colonization of calves and lambs by *Escherichia coli* O157:H7. *Infect. Immun.* **74**, 758–764 (2006).
9. Abe, A., Heczko, U., Hegele, R. G. & Brett Finlay, B. Two enteropathogenic *Escherichia coli* type III secreted proteins, EspA and EspB, are virulence factors. *J. Exp. Med.* **188**, 1907–1916 (1998).

10. Kaper, J. B., Nataro, J. P. & Mobley, H. L. Pathogenic *Escherichia coli*. *Nat. Rev. Microbiol.* **2**, 123–140 (2004).
11. Collins, J. W. et al. *Citrobacter rodentium*: infection, inflammation and the microbiota. *Nat. Rev. Microbiol.* **12**, 612–623 (2014).
12. Deng, W., Li, Y., Vallance, B. A. & Finlay, B. B. Locus of enterocyte effacement from *Citrobacter rodentium*: sequence analysis and evidence for horizontal transfer among attaching and effacing pathogens. *Infect. Immun.* **69**, 6323–6335 (2001).
13. Platenkamp, A. & Mellies, J. L. Environment controls LEE regulation in enteropathogenic *Escherichia coli*. *Front. Microbiol.* **9**, 1694 (2018).
14. Liu, B. et al. *Escherichia coli* O157:H7 senses microbiota-produced riboflavin to increase its virulence in the gut. *Proc. Natl. Acad. Sci. USA* **119**, e2212436119 (2022).
15. Pacheco, A. R. et al. Fucose sensing regulates bacterial intestinal colonization. *Nature* **492**, 113–117 (2012).
16. Rosay, T., Jimenez, A. G. & Sperandio, V. Glucuronic acid confers colonization advantage to enteric pathogens. *Proc. Natl. Acad. Sci. USA* **121**, e2400226121 (2024).
17. Jimenez, A. G., Ellermann, M., Abbott, W. & Sperandio, V. Diet-derived galacturonic acid regulates virulence and intestinal colonization in enterohaemorrhagic *Escherichia coli* and *Citrobacter rodentium*. *Nat. Microbiol.* **5**, 368–378 (2019).
18. Larzábal, M. et al. Early immune innate hallmarks and microbiome changes across the gut during *Escherichia coli* O157: H7 infection in cattle. *Sci. Rep.* **10**, 21535 (2020).
19. Langer, R. & Peppas, N. A. Advances in biomaterials, drug delivery, and bionanotechnology. *AIChE J.* **49**, 2990–3006 (2003).
20. Bernhard, S. & Tibbitt, M. W. Supramolecular engineering of hydrogels for drug delivery. *Adv. Drug Deliv. Rev.* **171**, 240–256 (2021).
21. Peppas, N. A., Hilt, J. Z., Khademhosseini, A. & Langer, R. Hydrogels in biology and medicine: from molecular principles to bionanotechnology. *Acta Mater.* **18**, 1345–1360 (2006).
22. Li, W. et al. Microfluidic fabrication of microparticles for biomedical applications. *Chem. Soc. Rev.* **47**, 5646–5683 (2018).
23. Majumder, P., Baxa, U., Walsh, S. T. R. & Schneider, J. P. Design of a multicompartment hydrogel that facilitates time-resolved delivery of combination therapy and synergized killing of glioblastoma. *Angew. Chem. Int. Ed. Engl.* **57**, 15040–15044 (2018).
24. He, F. et al. Controllable multicompartmental capsules with distinct cores and shells for synergistic release. *ACS Appl. Mater. Interfaces* **8**, 8743–8754 (2016).
25. Hu, Y. et al. Microfluidic fabrication and thermoreversible response of core/shell photonic crystalline microspheres based on deformable nanogels. *Langmuir* **28**, 17186–17192 (2012).
26. Yu, Y. et al. Microfluidic lithography of bioinspired helical micromotors. *Angew. Chem. Int. Ed. Engl.* **56**, 12127–12131 (2017).
27. Ding, Z. et al. Janus hydrogel microrobots with bioactive ions for the regeneration of tendon-bone interface. *Nat. Commun.* **16**, 2189 (2025).
28. Isabella, V. M. et al. Development of a synthetic live bacterial therapeutic for the human metabolic disease phenylketonuria. *Nat. Biotechnol.* **36**, 857–864 (2018).
29. Liu, M. et al. OptoLacI: optogenetically engineered lactose operon repressor LacI responsive to light instead of IPTG. *Nucleic Acids Res.* **52**, 8003–8016 (2024).
30. Krekhno, Z. et al. *Citrobacter rodentium* possesses a functional type II secretion system necessary for successful host infection. *Gut Microbes* **16**, 2308049 (2024).
31. Feuerbacher, L. A. & Hardwidge, P. R. Influence of NleH effector expression, host genetics, and inflammation on *Citrobacter rodentium* colonization of mice. *Microbes Infect.* **16**, 429–433 (2014).
32. Mao, T. et al. Hyaluronan-induced alterations of the gut microbiome protects mice against *Citrobacter rodentium* infection and intestinal inflammation. *Gut Microbes* **13**, 1972757 (2021).
33. Xie, L. et al. Effect of fecal microbiota transplantation in patients with slow transit constipation and the relative mechanisms based on the protein digestion and absorption pathway. *J. Transl. Med.* **19**, 490 (2021).
34. Sulaiman, J. E. et al. Elucidating human gut microbiota interactions that robustly inhibit diverse *Clostridioides difficile* strains across different nutrient landscapes. *Nat. Commun.* **15**, 7416 (2024).
35. Wiese, M. et al. 2′-Fucosyllactose inhibits proliferation of *Clostridioides difficile* ATCC 43599 in the CDi-screen, an in vitro model simulating *Clostridioides difficile* infection. *Front. Cell Infect. Microbiol.* **12**, 991150 (2022).
36. Yang, W. et al. Enterohemorrhagic *Escherichia coli* senses microbiota-derived nicotinamide to increase its virulence and colonization in the large intestine. *Cell Rep.* **42**, 112638 (2023).
37. Liu, Y. et al. 2′-Fucosyllactose and 3′-Sialyllactose reduce mortality in neonatal enteroaggregative *Escherichia coli* infection by improving the construction of intestinal mucosal immunity. *J. Agric. Food Chem.* **72**, 26165–26177 (2024).
38. Lynch, J. P., Goers, L. & Lesser, C. F. Emerging strategies for engineering *Escherichia coli* Nissle 1917-based therapeutics. *Trends Pharm. Sci.* **43**, 772–786 (2022).
39. Wang, Y. et al. The protective effects of 2′-Fucosyllactose against *E. Coli* O157 infection are mediated by the regulation of gut microbiota and the inhibition of pathogen adhesion. *Nutrients* **12**, 1284 (2020).
40. Wang, J. et al. 2′-Fucosyllactose ameliorates oxidative stress damage in d-galactose-induced aging mice by regulating gut microbiota and AMPK/SIRT1/FOXO1 pathway. *Foods* **11**, 151 (2022).
41. Dundas, S., Todd, W. T. A., Neill, M. A. & Tarr, P. I. Using antibiotics in suspected haemolytic-uraemic syndrome: antibiotics should not be used in *Escherichia coli* O157:H7 infection. *BMJ* **330**, 1209 (2005).
42. Zhang, C. et al. Structural modulation of gut microbiota in life-long calorie-restricted mice. *Nat. Commun.* **4**, 2163 (2013).
43. LoCascio, R. G. et al. Glycoprofiling of bifidobacterial consumption of human milk oligosaccharides demonstrates strain specific, preferential consumption of small chain glycans secreted in early human lactation. *J. Agric. Food Chem.* **55**, 8914–8919 (2007).
44. De Leoz, M. L. A. et al. Human milk glycomics and gut microbial genomics in infant feces show a correlation between human milk oligosaccharides and gut microbiota: a proof-of-concept study. *J. Proteome Res.* **14**, 491–502 (2014).
45. Kong, C. et al. Human milk oligosaccharides mediate the crosstalk between intestinal epithelial caco-2 cells and *Lactobacillus plantarum* WCFS1 in an in vitro model with intestinal peristaltic shear force. *J. Nutr.* **150**, 2077–2088 (2020).
46. Becerra, J. E., Yebra, M. J. & Monedero, V. An L-Fucose operon in the probiotic *Lactobacillus rhamnosus* GG is involved in adaptation to gastrointestinal conditions. *Appl. Environ. Microbiol.* **81**, 3880–3888 (2015).
47. Cheong, Y. E., Kim, J., Jin, Y.-S. & Kim, K. H. Elucidation of the fucose metabolism of probiotic *Lactobacillus rhamnosus* GG by metabolomic and flux balance analyses. *J. Biotechnol.* **360**, 110–116 (2022).
48. Cheng, L., Kong, C., Walvoort, M. T. C., Faas, M. M. & de Vos, P. Human milk oligosaccharides differently modulate goblet cells under homeostatic, proinflammatory conditions and ER stress. *Mol. Nutr. Food Res.* **64**, e1900976 (2019).
49. Liu, Y. et al. A fructose/H+ symporter controlled by a LacI-type regulator promotes survival of pandemic *Vibrio cholerae* in seawater. *Nat. Commun.* **12**, 4649 (2021).

50. Li, L. et al. Microbiota-derived succinate promotes enterohaemorrhagic *Escherichia coli* virulence via lysine succinylation. *Nat. Microbiol.* **10**, 749–764 (2025).
51. Robinson, C. M., Sinclair, J. F., Smith, M. J. & O'Brien, A. D. Shiga toxin of enterohemorrhagic *Escherichia coli* type O157:H7 promotes intestinal colonization. *Proc. Natl. Acad. Sci. USA* **103**, 9667–9672 (2006).
52. Johnson-Henry, K. C. et al. Short-chain fructo-oligosaccharide and inulin modulate inflammatory responses and microbial communities in Caco2-bbe cells and in a mouse model of intestinal injury. *J. Nutr.* **144**, 1725–1733 (2014).
53. Liu, Y. et al. *Vibrio cholerae* virulence is blocked by chitosan oligosaccharide-mediated inhibition of ChsR activity. *Nat. Microbiol.* **9**, 2909–2922 (2024).

Acknowledgements

This study was supported by National Natural Science Foundation of China (NSFC) Grants 825B2066 (to R.L.), 32170144 (to T.W.), 32470146 (to T.W.), 32100144 (to Y.L.), 32201183 (to G.T.), 82502737 (to X.L.); and National Key R&D Program of China grant 2024YFE0198900 (to Y.L.); Scientific Research Project of Tianjin Municipal Education Commission Grants 2024ZXZD016 (to M.Z.); China Postdoctoral Science Foundation Grant 2025M772657 (to X.L.); China Postdoctoral Science Foundation-Tianjin Joint Support Program Grant 2025T024TJ (to X.L.); Postdoctoral Fellowship Program of China Postdoctoral Science Foundation Grant GZC20251763 (to X.L.).

Author contributions

Y.L., T.W., G.T., and Y.S. designed the research; G.M., R.L., X.L., J.W.(Jialin Wu), Y.N., and S.W. performed the research; G.M., R.L., X.L., Z.C., X.Q., Q.W., J.W.(Junyue Wang), J.Q., M.Z., and Y.P. analyzed the data; and Y.L., G.M., R.L., X.L., and J.W.(Jialin Wu) wrote the manuscript. All authors gave final approval for the version to be published.

Competing interests

The authors declare no competing interests.

Additional information

Supplementary information The online version contains supplementary material available at https://doi.org/10.1038/s41467-026-69126-4.

Correspondence and requests for materials should be addressed to Yamin Sun, Guosheng Tang, Tao Wang or Yutao Liu.

Peer review information *Nature Communications* thanks Yun Yang, and the other, anonymous, reviewer(s) for their contribution to the peer review of this work. A peer review file is available.